20

Functional Connectivity of the Brain: Reconstruction from Static and Dynamic Data

ZOLTAN NADASDY, GYORGY BUZSAKI, and LASZLO ZABORSZKY

INTRODUCTION
THE BUILDING BLOCKS: NEURONS, CIRCUITRIES, AND ASSEMBLIES
- Classes of Neurons
- Basic Circuitry
- Vertical Organization of Circuitries
- Horizontal Organization of Circuitries
- Columnar Organization of the Neocortex
- Synaptic Reconstruction
- Cell Assemblies

STATIC DATA
- Connectivity Matrix
- The Importance of 3D Reconstruction
- Statistical Modeling
- Databases

DYNAMIC DATA
- Dynamic System Approach
- Large-Scale Recording of Neuronal Populations
- Reconstruction of Functional Connectivity
- Effective Connectivity

CONCLUDING REMARKS
APPENDIX
- Parametric Modeling of Neuroanatomical Data
- Databases
- Cross-Correlation Function

REFERENCES

ZOLTAN NADASDY • California Institute of Technology, Pasadena, CA 91125
GYORGY BUZSAKI AND LASZLO ZABORSZKY • Rutgers, The State University of New Jersey, Newark, NJ 09102

Abstract: The central nervous system is a single complex network connecting each neuron through a number of synaptic connections. However, only a small fraction of the total connections functionally link neurons together. If the smallest multineuronal architecture within which functional links are established constitutes circuitry, then what are the basic operating principles of these circuitries from which we can understand both the composition and the dynamics of the larger networks? We argue that a finite class of circuitries, the "basic circuitries," can be identified as repeating structural motifs tightly associated with specific dynamics. Functional circuitries, however, cannot be derived from the static architecture simply because they do not obey structural borders. Fortunately, since the constituent neurons do act in synergy, we can infer from the dynamics the minimal structural conditions that constitute a circuitry. In this chapter, instead of giving a precise definition of the "basic circuitry," we outline a set of methods that may elucidate such a definition. We argue that since the concept of circuitry incorporates both dynamic and static features, understanding can be achieved through combining the structural and dynamic aspects of the available data. We review methods of extracting functional information from static data first. Next, we review methods of extracting structural information from dynamic data. Ideally, these two approaches should converge and define circuitry based on the fragile concept of functional connectivity.

Keywords: cell types, circuitry, databasing, functional connectivity, large-scale recording, population statistics

I. INTRODUCTION

The ultimate objective of neuronal tract-tracing is to reveal the functional architecture of the nervous system. Progress toward this objective must rely on a precise definition of the architecture in order to successfully explain and predict the activity flow within its circuitries. This inferential process, however, is rather limited since the reconstruction or prediction of putative dynamics based on an abstract network architecture requires simulations that are extremely sensitive to small variations of a large number of parameters. Therefore, we propose that the coapplication of anatomical and electrophysiological methods is essential for describing a functional architecture of the nervous system. Although the inferential process of the electrophysiology and the neuroanatomy are quite opposite in nature, they support and complement each other. To find a link between them, we introduce the "structural and dynamic compactness" criterion, that is, to determine the smallest multiple-neuronal cluster, which generates the shortest invariant activity pattern. This practical definition of "circuitry" is sufficient to introduce the problem; however, further qualification and classification must go beyond the structural and temporal "compactness criteria," one of the key challenges of research for the next decade. This chapter will review constituent elements and main organization principles of cortical circuitries in the "The Building Blocks: Neurons, Circuitries, and Assemblies" section, specifically circuitries of the isocortex and the hippocampus will be discussed (both addressed as cortex). Next we discuss a number of innovative

applications of neuroanatomy and electrophysiology related to circuitries of the brain. We separately discuss methods related to morphological data in the "Static Data" section and physiological data in the "Dynamic Data" section. However, emphasis is put on the convergence and dialog between the two approaches in the "Concluding Remarks" Furthermore, we restrict our review to the rodent brain; however, the principles we outline can be generalized to the mammalian brain.

II. THE BUILDING BLOCKS: NEURONS, CIRCUITRIES, AND ASSEMBLIES

Despite the complexity and size differences between the invertebrate and the vertebrate nervous systems, both consist of large-scale repetition of compact architectural modules, which we denote as "basic circuitries." In order to define the basic circuitries within and across brains of different species, we first describe the constituent elements, the basic neuron types, and their specific connectivity pattern. The basic circuitry, which is uniform within a given brain structure, varies across different structures depending upon the computational needs. These basic circuitries, once we understand their dynamics, will enable us to infer the architecture from their activity pattern.

First, we need to make a distinction between structural and functional connectivity[1] and dynamics. The relationship between structural and functional connectivity is best understood if we decompose the large network of the nervous system into the smallest multineuronal information-processing subunit, or "motif." Motifs are conceived as small directed graphs of M-nodes within a large network. It has been shown through simulations that the number of structural motifs derived from anatomical connections of nervous systems in various species is smaller than that from random graphs (Sporns and Kötter, 2004). In direct contrast, when considering effective connections, real nervous systems show more functional motifs than do random graphs. This may suggest that the nervous system tends to maximize the number of functional motifs but minimize the number of structural motifs. However, when considering the diversity of activity patterns generated by networks of different functional motifs, it turns out that the number of dynamics is smaller than the number of functional motifs. Apparently, there is redundancy by which different functional motifs generate the same activity pattern (Prinz *et al.*, 2004). Therefore, dynamics may be more closely associated with architectures than to the functional connectivity. Defining circuitries by the dynamics they implement may allow us to reduce the necessary number of basic circuitries and simplify their classification. The price for this reduction is that the morphological composition of these circuitries may be rather complex.

[1] We also make a distinction between functional connectivity pertaining to connections between neurons as opposed to interareal connections inferred from functional imaging.

The prototypes of cortical circuitries are those that have been described in the hippocampus (Somogyi *et al.*, 1998). From architectural and developmental points of view, isocortical circuitries derive from the prototypical circuitries with a certain complexity added. Specifically, while the circuitries are relatively homogeneously distributed and coaligned in the hippocampus, the neocortical organization is complex and is conceived as an expansion of the hippocampal cytoarchitecture. This expansion involves three types of topological transformations. The first is a layer multiplication that adds a new set of interlaminar circuitries to the isocortex, nonexistent in the hippocampus. According to one view, the laminar structure of isocortex can be conceived as the unfolding of the hippocampus and superimposing of three subregions, the dentate, CA3, and CA1, as different layers but at the same time preserving the connections (Watts and Thomson, 2005). The second type of expansion of cortical development is a superposition of the same circuitry within the same cortical layer and often within the same volume, which makes reconstruction of the synaptic circuitry particularly difficult (Somogyi *et al.*, 1998). The third type of expansion is a radial specialization that forms columns and selective reciprocal tangential connections with functionally similar circuitries. This extension is responsible for creating the patchy functional architecture of the neocortex.

A. Classes of Neurons

Neuronal circuitries, at the lowest level, consist of two mutually exclusive classes of neurons, excitatory glutamatergic neurons (mainly pyramidal cells), and GABAergic inhibitory interneurons.[2] On the basis of an assessment from the CA1 area of the hippocampus, the pyramidal-to-interneuron ratio is 33:1 (Aika *et al.*, 1994). Principal neurons are the main excitatory projection neurons as they establish long-range connections and transfer information between different structures. In the cortex, pyramidal cells are reciprocally connected to the thalamus and to each other via axon collaterals. In spite of their diverse axonal projection patterns, pyramidal cells show a characteristic bipolar dendritic arborization which consists of apical and basal dendritic tufts. In contrast, most cortical interneurons incorporate a more diverse morphology. Interneurons establish differential reciprocal connections with other interneurons. The taxonomy of interneurons is still unresolved since the categories constructed based on histochemical staining, morphological features, termination sites, and firing patterns do not mesh. According to two extreme viewpoints on interneuronal diversity, cell types may either represent a finite set of discrete classes or blends of continuous feature distributions (Gupta *et al.*, 2000). Several inhibitory interneuron types have been classified solely based on morphological features, such as

[2] Among the few exceptions, the spiny stellate neurons in layer 4 are excitatory and considered interneurons.

basket, small basket, nest basket, axo-axonic, spiny stellate, aspiny stellate, Martinotti, double-bouquet, and a number of smaller classes (Gupta *et al.*, 2000). The inhibitory interneuron diversity seems to scale with the evolution of the mammalian brain. While brain structures with long evolution history, such as cerebellum, basal ganglia, and thalamus, consist of a few cell types, structures that specialized later, such as hippocampus and neocortex, show larger diversity. Moreover, interneurons show layer specificity in terminals (Freund and Buzsaki, 1996; Somogyi and Klausberger, 2005) and circuitry specificity. One speculation about interneuronal diversity is that it is the result of circuitry specialization. According to this view, GABAergic interneurons are added to the glutamatergic neurons to serve specific functional roles (Földy *et al.*, 2005). This is consistent with their different origin from pyramidal cells during the early development of the nervous system and a migration path orthogonal to that of the pyramidal cells (Rakic, 1995). The most accepted definition of interneuronal species takes several features into account, such as the postsynaptic target, the layer specificity, and the expression of species-characteristic markers (Freund and Buzsáki, 1996; Maccaferri and Lacaille, 2003; Somogyi and Klausberger, 2005).

B. Basic Circuitry

The next level of organization is the "basic circuitry."[3] All extrinsic and intrinsic glutamatergic pathways terminate on both pyramidal cells and GABAergic interneurons. Therefore, the basic circuitry is composed of pyramidal → pyramidal, pyramidal → interneuron, interneuron → pyramidal, and interneuron → interneuron functional units. The pyramidal–pyramidal excitatory connection is feed-forward if it connects two pyramidal cells between two areas or between subregions of the cortex (Fig. 20.1A). It is recurrent if axons project back to the same pyramidal cell population (Fig. 20.1B).[4]

Connections between neurons, in general, can be synaptic or electrically coupled (gap junction). Both pyramidal and interneurons can mutually connect through gap junctions that are instrumental for gamma and higher frequency band network synchronization. Interneurons seem to electrically couple only with the same subtypes (Gibson *et al.*, 1999; Tamás *et al.*, 2000). Conversely, connections between the same type of interneurons are often mutual, and the outcome of a steady-state input is an oscillation with zero-phase lag synchrony (empirical result and modeling: Destexhe and

[3] We would like to make a clear distinction between the concepts of basic circuitry and a "canonical microcircuit" of the neocortex (Douglas *et al.*, 1989). While the former denotes the basic information processing circuit involving only a few pyramidal and interneurons, the latter describes the basic architecture of an isocortical volume incorporating all six layers and all prototypical connections between the known neuron types.

[4] Very few autaptic axons, i.e., axons projecting back to the very same neuron, have been observed (Tamas *et al.*, 1997).

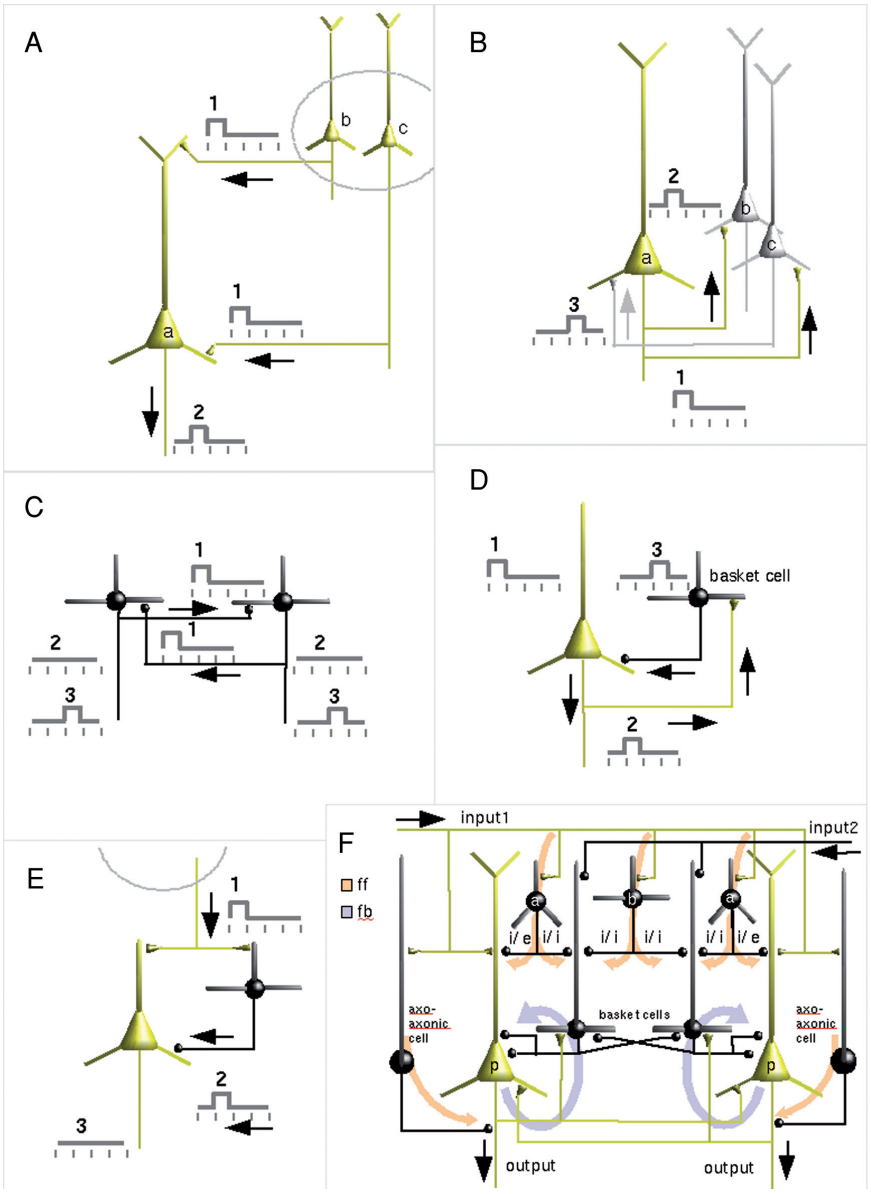

Figure 20.1. Most common examples of basic circuitry types. (A) Feed-forward excitatory connection involves excitatory projection from a different group of neurons (*b*, *c*) terminating on the target neuron *a*. The excitatory input from (*b*, *c*) must precede the action potentials in *a*. The relative timing of events is indicated by pulses and numbers. The flow of action potentials is indicated by arrows. (Examples: Schaffer collateral system in the hippocampus, layer 2–3 pyramidal → layer 5 pyramidal synapses in the isocortex.) (B) The recurrent or feedback excitation involves excitatory collaterals from *a* to other neurons of the same group (*b*, *c*). The excitatory input from *a* must precede the action potential in *b* and *c*, which in turn may cause a second

Babloyantz, 1993; modeling: Wang and Rinzel, 1993; Vreeswijk, 1996). The other main class of basic circuitry is the connection between projection neurons (pyramidal) and interneurons. Within an interneuron–principal cell couple, the interneuron controls the probability of the principal cell generating an action potential (AP) for a given excitatory input. The interneuron–principal cell connection can be feed-forward (Fig. 20.1E) or recurrent (feedback) (Fig. 20.1D). It is feed-forward if the interneuron, activated by an excitatory input, has an inhibitory effect on the target pyramidal neuron

←

Figure 20.1. (*Cont.*) wave of excitatory postsynaptic potential on neuron *a*. (Examples: Hippocampal CA3 recurrent collateral system, recurrent connections between layer 2–3 pyramidal neurons in the isocortex.) (C) Inhibitory–inhibitory connection between two GABAergic neurons. The sequence of action is important in order to understand how mutual inhibition causes oscillation with zero-phase-lag synchrony. When both neurons inhibit each other (phase 1), they both will be released from inhibition at the same time (Phase 2). Then they both elicit action potentials (Phase 3), which in turn cause them to be inactive for the next period, and the cycle starts over. Assuming sufficient depolarizing driving force, the phases of mutual inhibition and disinhibition generate a self-sustaining oscillation within the interneuronal network. (Examples: basket cells in hilus, layer 2–3 interneurons in the isocortex.) (D) Recurrent or feedback inhibition. In this case, the excitatory collateral projects to interneurons, which in turn project back to the same neuron. The recurrent inhibition is evoked by an excitatory input on the glutamatergic neuron (Phase 1), which generates an action potential. The action acts on the interneuron (Phase 2) through a collateral axonal projection, which in turn evokes an inhibition and when backprojected to the glutamatergic neuron (Phase 3) causes suppression of action potentials in the next phase. This type of control is effective to decrease the probability of action potentials of pyramidal neurons. (Examples: interneuron—pyramidal connections in the CA3 area of the hippocampus and pyramidal cell—basket cell feedback inhibition in the CA area of the hippocampus.) (E) Feed-forward inhibition. Distant excitatory inputs often projects to interneurons which terminate on local pyramidal cells. Functionally, the distant excitatory input (Phase 1) precedes the interneuron's response (Phase 2), which causes a suppression in the target pyramidal cells (Phase 3). A classic example of this circuitry is the lateral inhibition, common contrast-enhancement mechanism in sensory structures. Small black spheres are GABAergic terminals. Cone-shaped terminals are glutamatergic. Principal cells are shown in yellow, and interneurons are shown black. (F) A highly reduced model of isocortical circuitry can be conceived as the combination of above described feed-forward (orange) and feedback (viola) circuitries within a shared volume. This circuit repeats in each layer of the isocortex, often in juxtaposition and in superimposition with the same circuit within the same volume. Excitatory and inhibitory inputs are arriving on the top from left as input 1 and right as input 2, respectively. Only a single layer is featured. Connections between pyramidal neurons (p) and four different GABAergic interneuron types are illustrated. The laminar segregation of their terminals relative to the pyramidal cell is emphasized. Specifically, while the feed-forward inhibitory interneurons (*a* and *b*; such as double-bouquet, neurogliaform, and bitufted cells) preferentially target apical dendrites, the basket cells terminate perisomatically on the pyramidal neurons. Axo-axonic cell terminals, in contrast, occupy the axon initial segment. In addition, interneurons establish extensive and laminar interconnections amongst each other. The reciprocal excitatory–excitatory connections are also extensive. (After Somogyi *et al.*, 1998.)

prior to the common excitatory input activating the pyramidal neuron directly. The connection is recurrent if the interneuron, activated through recurrent axon collaterals, feeds back to the same pyramidal cell with a delay. Note that this morphological classification includes a dynamic criterion, the relative timing of the inhibitory and excitatory inputs. Accordingly, since pyramidal cells and interneurons are mutually interconnected within a region, whether inhibition is feed-forward or feedback can only be determined based on the relative timing of inhibition and excitation. Methods to resolve timing relationships will be discussed in Section 4C–D.

Different interneuron classes localize in specific hippocampal and cortical layers, and they establish connections with specific layers. Their axon termination is coaligned with excitatory input. In addition to their layer-specific distribution, different interneurons terminate selectively on specific parts of the pyramidal neuron. A highly simplified model of isocortical circuitry is shown in Fig. 20.1F. Only one excitatory and one inhibitory input is illustrated. Three basic types of interneurons are featured: axo-axonic, feed-forward inhibitory to excitatory interneuron (e.g., bistratified cell), and feed-forward inhibitory–inhibitory interneurons (e.g., basket cells). The feed-forward interneurons preferentially terminate on the apical dendrites and middle range dendrites. Basket cells are part of the feedback, feed-forward, and reciprocal inhibitions. Their terminals preferentially target the pyramidal cell soma. Axo-axonic cell terminals occupy the axon initial segment of pyramidal cells. The combination of convergent feed-forward and feedback connections effectively imposes a complex temporal pattern of inhibition on pyramidal cells through spatially segregated gating of the excitatory input from basal or apical dendrites (Fig. 20.1C). It is assumed that a concerted action of different types of interneurons is able to impose a complex temporal pattern of hyperpolarizations on the pyramidal cell (Somogyi and Klausberger, 2005).

C. Vertical Organization of Circuitries

Both the laminar arborization of the dendritic tree as well as the laminar organization of axons are cell-type specific. Furthermore, the efficacy of synapses on the postsynaptic cell is highly dependent on the spatial localization of the terminals relative to the postsynaptic cell's morphology. The closer the terminal is to the axon initial segment, the more effective is the inhibitory conductance. Therefore, inhibitory interneurons, such as the axo-axonic cells in the isocortex and the basket cells in the hippocampus, can effectively suppress the pyramidal cell response regardless of the excitatory postsynaptic potential, while interneurons terminating on the apical dendrite can suppress the integration of excitatory postsynaptic potential selectively for a specific dendritic cluster or branch.

Two examples of how basic circuitry types combine within the same volume to form a functional unit are shown in Fig. 20.2A. The first is a complex

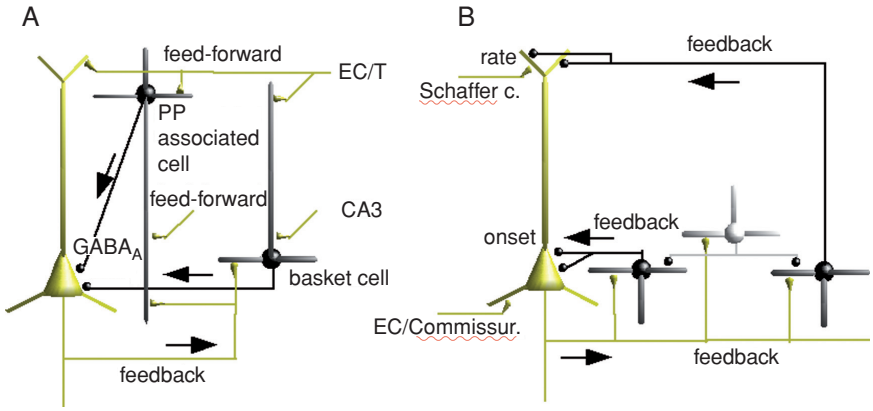

Figure 20.2. Hippocampal circuitries conceived as the composition of basic circuitries. (A) Combination of inhibitory feed-forward and feedback circuitries. The feed-forward circuitry is established through excitatory input connections from entorhinal cortex or thalamus terminating on perforant path (PP) associated cells that inhibit pyramidal cells near the soma. This is convergent with the recurrent inhibition through basket cells that are coaligned with the Schaffer collateral/comissural input and also terminate perisomatically. The design of the two convergent but spatially segregated inhibitory sources suggest coordinated inhibition on the pyramidal cells. (B) Another example of the hippocampal CA1 circuitries where the in vitro physiological response has been clarified. Spatially segregated recurrent (feedback) inhibition circuitries originate and act on the same pyramidal neuron. One is acting on the apical dendrites, the other is perisomatic. During stimulation through alveus, the inhibition rapidly shifts from the soma to the apical dendrites. While the somatic inhibition acts in a time-dependent fashion, the distant dendritic inhibition is prolonged and frequency dependent (Pouille and Scanziani, 2004).

feed-forward/feedback circuitry of hippocampal CA1 pyramidal cell, basket cell, and perforant-path-associated cell. Basket cell terminals are coaligned with the Shaffer collateral or comissural input, while the perforant-path-associated interneuron is coaligned with the entorhinal/thalamic input. The combination of the two types of inhibition, feed-forward and feedback, exerts an effective control over the integration in the pyramidal cell as they both act on the soma (Somogyi *et al.*, 1998). The other example, representing a combined feedback inhibition, is also from the CA1 area of the hippocampus (Fig. 20.2B). By using simultaneous somatic and dendritic recordings in vitro, a rapid shift from somatic feedback to dendritic feedback inhibition can be observed (Pouille and Scanziani, 2004). The somatic feedback most likely acts via basket cells. These observations suggest that two spatially disjoint circuitries process input onset time and prolonged rate in the same pyramidal cells separately. This simple circuitry, by utilizing the somatodendritic dynamics of inhibition, may enable pyramidal cells to allocate separate channels for processing time-encoded and firing-rate-encoded information.

From the layer specificity of dendritic and axonal distributions, one can derive quantitative models of circuitries. Even if synapses are not available for direct observation, one can estimate the number of synaptic contacts by applying Peters' rule (Peters and Feldman, 1976). Consider, for example, a cortical volume traced for two types of neurons, type i and type j. According to Peters' rule, given S_j^u the number of synapses in cortical layer u established by presynaptic neurons of type j, the number of neurons in layer u, and D^u the summed length of all dendritic branches in layer u, one can calculate the number of synapses S that all neurons of cell type j establish with the apical dendrite of neuron i:

$$S_{ij}^u = S_j^u d_i^u / D^u.$$

This formula is based on the assumption that synapses distribute evenly. Applying this formula, Binzegger *et al.* (2004) were able to calculate the number of synapses between inhibitory and excitatory neurons in the primary visual cortex of a cat. The calculation led to a few surprising revisions of the traditional circuitry diagram of area 17 (Gilbert, 1983; Gilbert and Wiesel, 1983; Szentagothai, 1978). For example, the most important circuitry in area 17 was believed to consist of a high-bandwidth sensory feed-forward pathway of X/Y afferents, originating from the dorsal lateral geniculate nuclei (LGN) and terminating in layer 4 spiny stellate cells. What changed this view was taking into consideration that layer 4 cells establish massive excitatory connections with layer 2/3, 5, 6 pyramidal cells and feedback to layer 4 through a recurrent loop. Based on a quantitative assessment of the synapses, it became evident that the feed-forward pathway comprises only 21% of all excitatory connections (Binzegger *et al.*, 2004). In contrast, at least 34% of connections are intrinsic, i.e., establishing long-range horizontal connections within the given layer and interconnecting different columns (Fig. 20.3). Similar relationships were found among inhibitory–inhibitory and inhibitory–excitatory neurons.

The selectivity of excitatory and inhibitory connections appears to be circuitry and layer specific within the same cortical area. For example, feed-forward projections from pyramidal neurons preferentially target other pyramidal neurons; however, feedback connections mainly target interneurons (Watts and Thomson, 2005). More specifically, feed-forward projections from layer 4 to 3 and from layer 3 to 5 target pyramidal cells and to lesser degree interneurons. "Feedback" projections from layer 5 to 3 and from layer 3 to 4, on the other hand, mainly target interneurons.

Using one of the most powerful techniques, optical release of caged glutamate in combination with intracellular or multiple extracellular recordings, Callaway and colleagues demonstrated an intracolumnar fine-scale organization of layer 2/3 cortical neurons (Yoshimura *et al.*, 2005). Specifically, adjacent pairs of layer 2/3 pyramidal neurons that are connected to each other share common input from layer 4. Conversely, those that are not connected share negligible input. In contrast with this fine-scale specificity, inhibitory or layer 5 excitatory input are all shared across layer 2/3 cells,

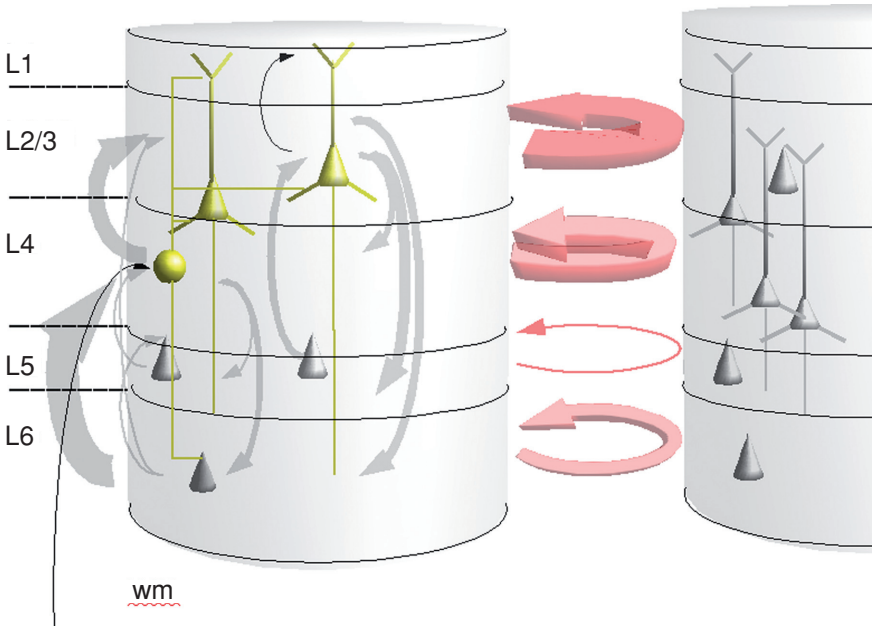

Figure 20.3. The cortical circuitry of excitatory connections based on synapse density in cat visual cortex area 17 (Binzegger *et al.*, 2004). The cylindrical volumes represent cortical columns. Arrows are the local excitatory connections. The arrow thickness is proportional to the number of synapses (total number of synapses between excitatory neurons = 13.6 × 1010). Gray arrows represent connections between layers. Pink arrows are within layer connections. Some of these connections project from other columns. Note that the within layer excitatory connections outnumber the feed-forward sensory connections (cortical layers numbered; wm, white matter).

regardless of whether they are connected or not. Whether this example of a layer-specific fine-scale organization of neurons represents a functional subnetwork independent of columnar compartmentalization remains to be investigated.

D. Horizontal Organization of Circuitries

We must make a clear distinction between the vertical specialization of circuitry and the horizontal (short and long range) associational connections. These associational connections interconnect different vertical circuitries, regardless of whether these circuitries cluster according to columns or not. The range of these horizontal connections vary from adjacent columns (50–200 μm) to different cortical areas or different hemispheres (few centimeters). Excitatory associational long-range connections localize broadly between layer 3 and layer 6. Horizontal excitatory axon collaterals and interneurons from layer 3 arborize in "patches" at distant excitatory targets

within layer 2/3 and 5. Furthermore, excitatory long-range connections originate from layer 5 where local ascending connections also derive. Layer 6 pyramidal cells also send long-range horizontal and oblique collaterals.

Starting with the short-range horizontal connections, pyramidal cells in cats' and monkeys' primary visual cortex (V1) send excitatory axons to neighbor columns. Whether target specificity is selective with respect to orientation columns is not clear. According to a study by Das and Gilbert (1995), spikes from the neuron's cell body spreading in a radius of 400–1100 μm radius and subthreshold activation extending as far as 3.2 mm in cat V1 preferentially target columns with similar orientation. In contrast, the same authors found by measuring correlation between neuron pairs located in optically imaged maps of V1 orientation columns that the strength of local connections between cells is a graded function of lateral separation across cortex, largely radially symmetrical and relatively independent of orientation preferences (Das and Gilbert, 1999). Collinear facilitation observed between pyramidal cells with nonoverlapping receptive fields supports a key role in contour integration (Li and Gilbert, 2002).

Complementary to excitatory connections, local inhibitory interneurons may substantially contribute to the functional segregation and dynamic assembly of orientation columns. Selective suppression of different orientation domains of adjacent columns may enhance the contour integration. The first important difference between lateral inhibitory and excitatory connections is that inhibition has a shorter (250–500 μm) radius. Morphological reconstruction of large GABAergic basket cell axonal arborization and superposition on local orientation maps obtained by optical imaging have revealed selective targeting. Specifically, visual area 17 layer 4 clutch cells (a subtype of basket cells) arborize isotropically near their cell body within 50 μm, restricted to the nearest adjacent columns (Budd and Kisvarday, 2001). However, axons beyond this core show highly domain-specific topography (Kisvarday *et al.*, 2002).

The long-distance horizontal connections, which extend beyond specific cortical subregions, form a massive cortico-cortical network. Probably the best studied such interareal network is the visual pathway where the most complete functional connectivity map is available. This map revealed a network of distributed hierarchical processing (Felleman and Van Essen, 1991) based on the systematic mapping of long-range cortical associational connections that have been published during the last few decades. It illustrates the enormous effort to extract connectivity information from published data. Mapping associative connections between other cortical areas, such as the prefrontal cortex (Kötter *et al.*, 2001; Rempel-Clower and Barbas, 2000), is in progress. This type of mapping involves a combination of retrograde tracing with electrophysiology because the range of connections is at the super millimeter level and cannot be tracked from the same section. High-resolution functional and optical imaging applying voltage-sensitive fluorescent dyes with confocal or two-photon microscopy may substantially facilitate the functional verification of the connections, especially the horizontal

associational and callosal connections (Chen-Bee *et al.*, 2000; Grinvald and Hildesheim, 2004; Petersen, in this volume).

E. Columnar Organization of the Neocortex

The organization module that integrates both vertical and horizontal connections is the cortical column. The concept of columnar architectonics of the cerebral cortex arose originally from the early physiological observations of Mountcastle (1957) of the vertical columnar organization of the somatosensory cortex. This was soon followed by an analogous architectural principle in the visual cortex found by Hubel and Wiesel (1959). The columnar architectonic principle of the cortex has received crucial support from studying the callosal and associational connections in primates by Goldman and Nauta (1977). The arborization spaces of callosal columns are one order of magnitude larger (300 μm–3 mm) as compared to the orientation columns of Hubel and Wiesel (1972). Even after transections of large parts of the corpus callosum, the distribution of degenerated fibers shows a discontinuous pattern: in coronal sections hourglass-shaped territories containing massive degeneration are alternating with areas containing little or no degenerated terminals (Zaborszky and Wolff, 1982). Cortico-cortical associational connections show inhomogeneous distribution pattern similarly to callosal columns (Zaborszky, 2002). The systematic studies by Burkhalter, Killackey, Malach, and more recently by Sakman and their colleagues (Coogan and Burkhalter, 1993; Johnson and Burkhalter, 1997; Koralek *et al.*, 1990; Lubke *et al.*, 2000; Malach, 1994; Paperna and Malach, 1991) in the rodent cortex and that in the prefrontal cortex in primates by Patricia Goldman-Rakic, Helen Barbas, and David Lewis (Barbas and Rempel-Clover, 1997; Goldman-Rakic, 1984; Pucak *et al.*, 1996) amply confirmed the columnar nature of associational connections that can be utilized to predict the hierarchical organization of cortico-cortical connections as shown in the often cited diagram of Van Essen (Felleman and Van Essen, 1991). The size of associational columns in primates compared with the size of the associational columns in rats show a remarkable congruence.

The idea of columnar organization of the neocortex[5] is part of a more general hypothesis of modular organization of the nervous system, a widely documented principle of design for both vertebrate and invertebrate brains (Szentagothai, 1983). Some of the main characteristics of the modular principle are summarized in a review by Liese (1990) and in a superb book on the anatomy and functions of cerebral cortex by Mountcastle (1998). The following features can be enlisted: (1) Modules are local networks of cells in any region of the CNS, containing one or more electrically compact

[5] A more detailed discussion of the columnar–modular organization of the cortex is beyond the scope of this chapter and the reader is referred to a recent review by Rockland (1998).

circuits active in a particular behavioral function. (2) Modules are dynamic entities—modules, repeated iteratively within each larger structure, function independently, or they may act together when combined in groups whose composition may vary from time to time. (3) Modules may differ in cell type and number in internal and external connectivity and in the mode of neuronal processing between different large entities; but within any single entity, like the neocortex, they have a basic similarity of internal design and operation, ranging in diameter from about 150 to 1000 μm. (4) The neighborhood relations between connected subsets of modules in different entities result in nested systems that serve distributed functions. A cortical area defined in classical cytoarchitectural terms may belong to more than one and sometimes to several such systems. (5) Modules may develop through ontogenesis and phylogenesis by duplication of homeobox genes (Allman, 1998).

Modules can often be anatomically differentiable from surrounding tissue, for example, associational or callosal columns in the cortex using tracing methods, the striosome–matrix compartments in the striatum using AChE histochemical reaction (Graybiel and Ragsdale, 1978), or the application of immunocytochemical and autoradiographic methods for the presence of various transmitters and receptors (Gerfen, 1985). AChE staining also delineates patches in the superior colliculus that represent special sites where information from various sensory modalities can be integrated (Chevalier and Mana, 2000). In other brain regions, such as the auditory nuclei (Malmierca *et al.*, 1998), the pontine gray (Leergaard *et al.*, 2000), or the basal forebrain (Zaborszky *et al.*, 2005b), computational anatomical methods helped to reveal a clustered, putatively modular organization, defined by patterns of connectivity. For the historical record, we reprint here in Fig. 20.4 Szentagothai's imaginative models about cortical modules in which he envisioned to place the elementary circuitries of the neocortex in repetitive spaces of callosal columns.

F. Synaptic Reconstruction

Precise assessment of the number of synapses has been done entirely by using electron microscopy (EM) in 2D sections (see Avendano, this volume). Full 3D reconstruction of neurons based on EM has only recently became available (Fiala and Harris, 2001; see also the chapter by Duque and Zaborszky, this volume). As a shortcut, using the correlation between dendritic spines and synapses, it is possible to estimate the number of synapses based on two-photon microscopic reconstruction of neurons (Yuste and Denk, 1995) and investigate the specificity of synaptic connections relative to random dendritic contacts (Kalisman *et al.*, 2005). These measurements provide the most reliable quantitative assessment that could guide further calculations on the bandwidth at different components of the circuitry, thus allowing reconstruction of the functional connectivity.

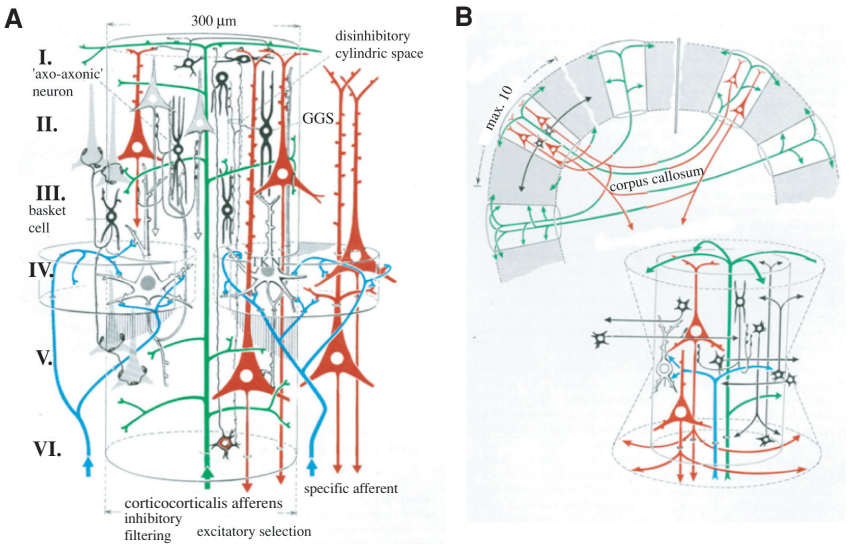

Figure 20.4. The callosal and associational columns. (A) Arrangement of neurons and local circuits in one cortical columnar module. Pyramidal cells: red; specific afferents: blue; corticocortical afferents: green; inhibitory neurons: solid black; TKN: spiny stellate excitatory neuron; GGS: inhibitory neuron (double-bouquet cell of Cajal) connected to other inhibitory neurons. The effect of the Martinotti cell in L VI spread upto L I. (B) Interconnections of associational and callosal columns. The output of each column originates from pyramidal cells, their terminal axonal arborizations are labeled green. Ipsilateral connections maximally up to 10 columns. The lower right scheme shows some of the dynamic features: in L I and VI the excitation expands the diameter of the column, in L IV, the inhibition shrinks the cylinder (Reprinted with permission from Szentagothai and Rethelyi, 2002.)

Combining voltage-sensitive Ca^{2+} imaging with two-photon microscopy it was possible to monitor activity of 100–1000 neurons from a 150 × 150 or 300 × 300 µm cortical volume of area 18 in cat and rat in vivo at a < 1-µm spatial resolution, allowing unambiguous cell body identification (Ohki *et al.*, 2005). By improving the stability and signal-to-noise ratio of the voltage-sensitive dyes, the temporal resolution of this technique can be reduced to sub-second rates to achieve a dynamic imaging of whole populations of neurons simultaneously.

For submicroscopic structures, such as gap junction, EM verification remains to be necessary (Fukuda and Kosaka, 2000). However, the combination of precise morphology-based modeling with physiological level simulations allows predictions about network dynamics to be made. For example, multicompartmental modeling of the cellular morphology of interneurons and pyramidal cells, including the number of synapses and various input currents, led Traub *et al.* (1999) to conjecture that gap junctions are necessary for high-frequency synchronization, commonly observed in the hippocampus and neocortex.

G. Cell Assemblies

The next level of organization is the cell assembly level (Hebb, 1949; Wickelgren, 1999). Although the original definition of cell assembly was purely conceptual, the empirical definition relies on both structural and dynamic criteria. Structural criteria are the "overlapping set," "sparse coding," and "high density of excitatory connections," and the dynamic criteria are "persistence," "completion," and "Hebbian learning." The morphological substrate of cell assemblies and the mechanism by which neurons dynamically form functional groups are still undetermined. In general, a cell assembly represents a coalition of neurons within which neurons act in a synergistic fashion. These coalitions can be established in a topological or a topographical basis in the spatial domain, as well as dynamic or static basis in the temporal domain. Neurons with correlated activity are likely to group together during development and form a topographically compact network. This type of cell assembly is static and supports stable functions over a period of time. The other type of cell assembly is dynamic and may not segregate into topographical cell clusters. This is typical in structures supporting flexible associative function between cells such as the hippocampus (Harris *et al.*, 2003) or interface structures with a large input/output divergence (higher sensory cortical areas). While topographical cell clustering is not a defining feature of cell assemblies, temporal synergy is. On the other hand, since temporal synergy often derives from the common input to the constituent neurons, topographical and temporal compactness are usually codetermined. Temporal compactness can be detected as coherence, while spatial compactness is a morphological feature. Since cells with overlapping dendritic arborization are likely to share input, they must respond to the common input with a synergistic fashion (see section "Statistical Modeling"). However, temporal compactness can be derived from the high interconnectedness of a group of neurons that generate the same spike pattern regardless of the input. Therefore, cell assemblies created by the common input must be distinguished from cell assemblies formed by the synergy of neurons. To consider all these possibilities of neuronal ensemble formation, one needs to combine anatomy with physiology. Fortunately, the combination of morphological and dynamical features results in a finite set and, as we argue, the lexicon of connection patterns and dynamics fall into several categories. For example, neurons with overlapping dendritic trees sharing a common input can either form a feed-forward or a recurrent network. If the output of these cells reliably reflects the temporal structure of the input, then the network is feed-forward, otherwise it is likely to be recurrent.

The ability to record simultaneous activity from a population of identifiable neurons brings up important questions concerning the relationship of anatomical connections between neurons ("structural connectivity"), the observed correlations between the activity of different neurons ("functional connectivity"), and the causal sequence ("effective connectivity"). It has been considered for many years that several neuronal configurations are

compatible with the same observed firing correlations leading to the concept of a simplest "effective" mechanism that can account for the data (e.g., Aertsen *et al.*, 1989). Furthermore, the same observed activity pattern recorded from a group of neurons may be underlain by different network connectivity, suggesting that the robustness and self-organization of activity patterns are more important than the precise architecture (Prinz *et al.*, 2004). Much further work will need to be done before we can unequivocally specify the relationships between structural and functional connectivity, the number of their distinct configurations, and the potential benefit of redundancy at any of these levels.

III. STATIC DATA

A. Connectivity Matrix

The static architecture of neuronal information processing relies on the map of connectivity, i.e., the connectivity matrix. We will refer to this as "static connectivity" in contrast with the "functional connectivity," which represents active connections, equivalent with the map of information flow, defined by measuring spike-train to spike-train correlations (see section "Dynamic Data"). Theoretically, one can construct an immense matrix including all neurons as i indices and list the same neurons as j indices to represent all the monosynaptically connected neuron pairs with the number of synapses. Within this matrix, we should find numerous isolated hot spots representing major hubs and symmetric blocks indicating long-range connections as well as local reciprocal connections. More detailed analysis of the matrix would resolve the primary associations between basic neuron types (e.g., association of Purkinje and mossy cells in the cerebellum, or basket cells and granule cells in the dentate area of the hippocampus), those that we have described as circuitries. The next level of associations would indicate static assemblies, those that represent functionally related groups, such as ocular dominance columns of the visual cortex, barrels in the somatosensory cortex of the rat, or glomeruli of the olfactory bulb. The next level of associations would reveal brain regions, such as the thalamus, hippocampus, colliculus-superior, etc., including functionally distinct cortical areas. To construct such a matrix is beyond the current technological capabilities and may not be feasible at all. However, what is technically feasible is the regional mapping of connections. We refer to this as the connectivity map, a small part of the theoretical connectivity matrix limited to a specific structure. This is within a reach of the current technology, since a database like this could be developed incrementally (see section "Databases"). Detailed regional mapping and tracing of connections of various brain areas over a century have revealed the critical organizational features of these structures allowing to make generalizations and construct accurate models (see chapter by Ascoli and Scorcioni, in this volume).

B. The Importance of 3D Reconstruction

In order to create connectivity maps, first one has to identify the elements of connections, such as dendrites, axons, spines, and synapses. There are two basic approaches of extracting these structures from histochemically prepared slices. Both approaches are based on human operators to recognize these elements; however, data registration has been substantially accelerated by computer technology. One is based on image analysis and the other is based on vectorial tracing. Both methods start with application of specific markers (Amunts and Zilles, Ascoli and Scorcioni, and Bjaalie and Leergard, this volume). The goal of image analysis is to recognize elements of connections from images. To date, there are a number of image-enhancement methods, such as edge detection, contrast enhancement, and texture analysis, that can aid or make the recognition of different structures unsupervised (He *et al.*, 2003; Rodriguez *et al.*, 2003).

The other approach derives from the technique of camera lucida, which is based on manual tracing of outlines under the microscope at different levels of details, including cellular, population, and structure level. Originally, this method was introduced to trace the contours of cells and connections with maximal precision. Today, under computerized microscope control, the tracing of individual sections is still done by an operator; however, traces are registered with their X, Y, and focal depth coordinates to a database by computer. The computer encodes each contour segment by a vector in the 3D Cartesian coordinate system in addition to the coordinates indexed by the actual section under the microscope. By combining these sections, we can reconstruct the virtual 3D structure of an entire traced neuronal system. The reconstruction may involve interpolation between adjacent sections unless the sectioning was gapless. The result is a 3D vectorial representation of the cells that may include, besides cell bodies, the corresponding dendritic processes and eventually axons. One major advantage of 3D representation in a Cartesian coordinate system is that it enables one to view the data from different angles and virtually zoom in to any level of detail. Furthermore, using a standard stereotactic coordinate system, the 3D representation allows incremental development of a database by adding new elements. The most widely adopted commercial system for vectorial data acquisition is MicroBrightField's Neurolucida® (MicroBrightField Inc., VT; see Ascoli and Scorcioni, this volume).

The two types of data representation, image and vector, are fundamentally different and combining them is a major challenge in developing neuroanatomical databases for the future. Although the 3D vectorial representation is better suited for tracking neural processes across sections than the image format, it does not automatically identify the connections. Synaptic connections can only be verified with EM or physiology. Therefore, connections revealed by light microscopy are only putative and inferentially based on a set of critical attributes. These attributes are synaptic boutons, dendritic spines, or the proximity of axons and dendrites. A less reliable but

still useful attribute is the overlapping dendritic arborization that indicates shared input source since en passant axons are likely to establish contact with all neurons with overlapping dendritic arbors.

Ideally, for a population database, one would like to map neurons along with their cell body, dendrites, and axons in relation to other neurons and structure outlines or other available morphological markers, such as cortical layers. Axons, however, are difficult to trace due to their small diameter and that they may traverse across multiple sections and depth planes. However, an intermediary solution for reconstruction of the axonal tree is to scan camera lucida paper-and-pencil drawings and apply an algorithm that follows a nearest-neighbor strategy (Ascoli and Scorcioni, this volume). Because the connectivity is not readily available from tracings, reconstruction of the *connectivity map* of large populations of neurons requires using a few inferential heuristics. Such heuristics are the following: (a) neurons that group together are likely to be functionally related; (b) neurons with overlapping dendritic arborization are likely sharing input; (c) spatial association of chemically identified cell types reflects functional synergy. Guided by these heuristics, methods have been developed to extract and visualize hidden association of neurons (Stepanyants *et al.*, 2004). The first group of methods is based on cell body distribution; the second is based on dendritic morphology.

C. Statistical Modeling

When a population of cell bodies have been selected with an unbiased sampling, traced, and registered in 3D, a valid question is whether the distribution of neurons suggests a pattern that further implicates functional relatedness. Obviously, the anatomical relationship is only suggestive and a functional relationship must be tested by physiological methods. The null hypothesis (H_0) is that neurons distribute evenly within the volume of interest. In contrast, if neurons cluster, we need to reject H_0, which again does not necessarily imply any functional relatedness among neurons of the same cluster. One algorithm of testing for homogeneity is the following:

1. For digitization, design a set of grids with linearly increasing grid sizes. This grid serves to partition the total volume of interest into voxels.
2. Apply the largest grid size that is smaller than the smallest possible cluster size.
3. Count the number of cell bodies within each voxel. Cell counts represent local densities.
4. Impose a density threshold. Voxels with local density larger than threshold can be visualized by surface rendering.
5. Employ the next larger grid size and recursively apply steps 3–5 until the grid is larger than the largest possible cluster size.

If H_0 is correct, then the average cell density within the filled voxels should increase linearly (that is, the total number of cells within the filled

voxels should increase exponentially) with the grid size, while the number of filled voxels should also increase linearly. Deviation from the linear density change, for example, a stepwise increase in average cell density, indicates inhomogeneity. The precise cell density and grid size at which the largest stepwise increase of density occurs is the one that corresponds to the critical density and cluster size, respectively. This algorithm was applied to reveal hidden clustering of cell bodies within the basal forebrain cholinergic system (Nadasdy *et al.*, submitted; Nadasdy and Zaborszky, 2001; Zaborszky *et al.*, 2002, 2005b). Having the critical density and size determined, one can apply a grid size that fits to the cluster size and compute the local cell density within the voxels constructed by this grid (Fig. 20.5B). Next, select only those voxels where the density is equal to or larger than the critical density. These voxels delineate putative neuronal clusters (Fig. 20.5E). To visualize these clusters, apply a surface rendering on the selected voxels. To eliminate sharp edges between adjacent polygons, it is recommended to interpolate and smoothen the polygons before surface rendering is applied (Fig. 20.5F). For construction of volumetric database and isodensity surface rendering, see the Appendix..

Visualization of such clusters can place these clusters into the context of the macro-architecture (Fig. 20.5D–F). We can take the density analysis one step further and apply it to the association of different cell types. For example, if the brain sections were histochemically stained for choline acetyltransferase, parvalbumin, calretinin, and calbindin, then each of these markers will label a subpopulation of neurons specifically associated with a specific cell type. These populations can be considered either as four independent spatial distributions (H_0) or a coordinated distribution of four markers (H_A). One could ask the following question: Knowing the spatial distribution of each marker population, what is the probability of finding a parvalbumin and a cholinergic neuron within the same voxel by chance? The combined by-chance probability is the product of the local probabilities of occurrences of the two markers. If the observed coregistration probability is larger than the expected by-chance coregistration of markers, then we must reject H_0. Rejection of H_0 does not necessarily imply functional relatedness. Nonetheless, assuming that neurons within the same density cluster share common input, H_A is suggestive of a functional association of different cell types (Zaborszky *et al.*, 2005b).

Dendritic morphology, when combined with cellular density data, further supports the inference from the spatial distribution to the connectivity map. Utilizing the overlapping dendritic volume as an indicator for shared input provides an additional attribute of functional cell clusters. To explore this option, we used a large database of basal forebrain cholinergic neurons ($n = 15{,}700$ neurons) and extracted an unbiased random sample of 750 neurons for dendritic morphology tracing. Next, we determined the 3D orientation of the main axis of the dendritic tree and, for each individual cell, we replaced the dendrite with a vector pointing from the cell body. The vector's orientation was identical to the orientation of the dendritic

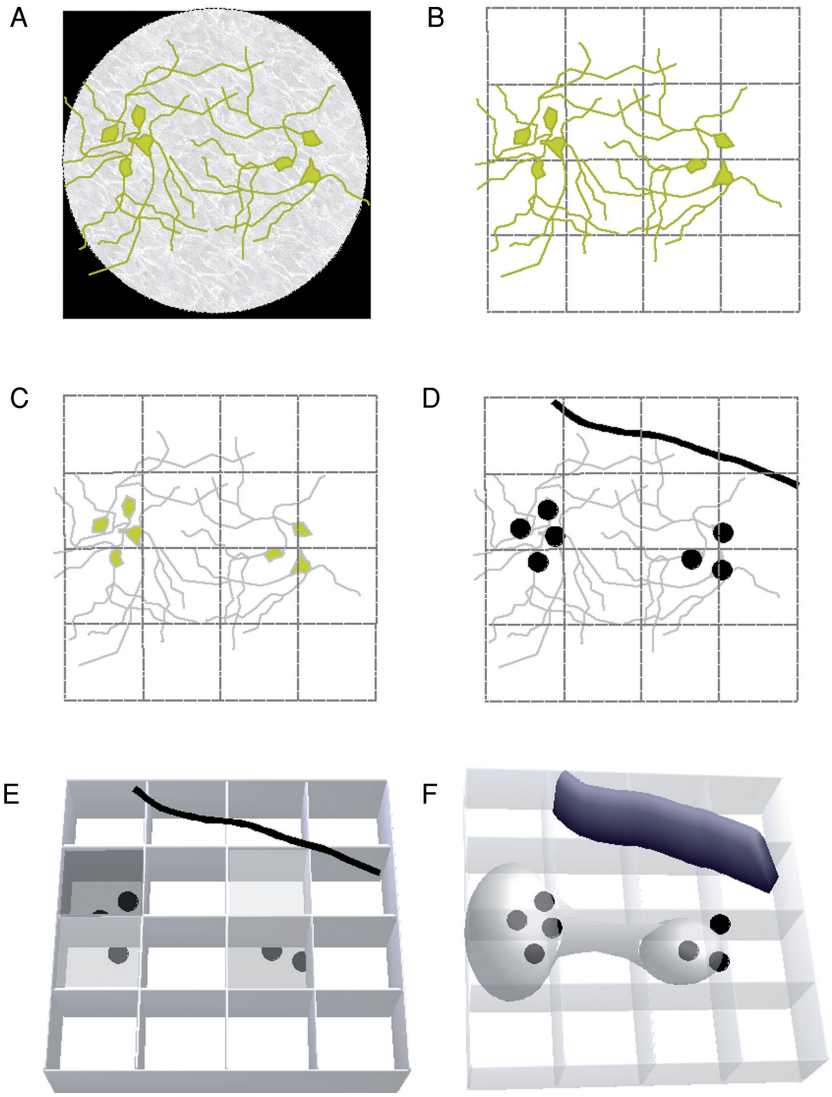

Figure 20.5. Visualization of neuron clusters by using isodensity surface rendering. (A) Microscopic image of immunohistochemically labelled neurons. (B) Camera lucida reconstruction of neuron outlines with processes. (C) A grid is defined that incorporates the size of clusters to be determined. Cell bodies are highlighted. (D) Cell bodies enter with their voxel coordinates. (E) The number of cell bodies within each 3D grid is determined and the local density is assigned to each voxel. (F) Voxels at which the density exceeds a certain threshold create a volume. This volume, encompassing the spatial structure of neuron clusters, can be visualized by surface rendering and superimposed on clusters obtained from other cell markers.

volume, estimated as the center of dendritic mass relative to the cell body, and vector length was proportional to the dimension of the dendrites. Here, one can use a different abstraction of parameters. The vector can represent dendritic length, dendritic density, dendritic volume, etc. Alternatively, instead of a single vector one can apply two vectors that better describe bipolar dendritic arborizations. The importance of dendritic vector abstraction is twofold. First, it allows one to estimate the overlapping of the volume that a dendritic tree can sample, thus providing a quantitative assessment of the shared input. Second, proportional enhancement of vectors allows a visual representation of the dendritic orientation pattern in the context of the cellular distribution pattern, which otherwise would not be seen at a true microscopic scale. When neurons represented with their dendritic vectors were projected to a 3D coordinate system and visualized relative to the outlines of the cholinergic column, the dendritic orientation revealed a systematic pattern (see Fig. 5 in Zaborszky *et al.*, 2002). Along the septal cholinergic volume, a spiral staircase pattern of dendritic orientation was observed that was orthogonal to the orientation of the septal column. This architecture suggested an optimal sampling of the en passant axons parallel to the septal column (Somogyi *et al.*, manuscript in preparation.

Although synapses with their respective postsynaptic target can reliably be identified only by EM, the presence of synaptic marker proteins such as synaptophysin or ProSAP2/Shank3 can give an estimation of synapses at the population level using light microscopy. Also, using a tour de force confocal regimen (see Wouterlood, this volume) putative synapses from 3D reconstructions can be determined. Using different proximity scales, Stepanyants and colleagues determined the number of "graphical" contacts, i.e., the potential synapses, between overlapping dendritic and axonal segments. Next, they shifted the coordinates of the dendritic arbor in silico by ~30 μm (Stepanyants *et al.*, 2004) to establish a different set of potential synapses. Their rationale was as follows. If the axons and dendrites establish contacts on a by-chance basis, the shift should not affect the number of potential synapses. By varying the shifts, it was possible to determine the necessary shift beyond which the misalignment destroys the potential synapses to the by-chance level. The precision at which axons establish potential synaptic contacts was found to be consistent within the shaft dimension (0.4 μm) and dendritic spine dimension (2.0 μm) (Stepanyants *et al.*, 2002, 2004). Considering this metric, it was also evident that the number of actual synapses represent only 10–30% of the potential synapses, indicating significant room for plasticity to convert potential synapses to actual. Exploration of the regional and laminar differentiation of potential synaptic contacts will hopefully elucidate further details of cortical circuitries. The use of computational and statistical methods could play a major role in exploiting the richness of data available from the 3D morphology and population scale reconstruction. Therefore, systematic construction and incremental combination of morphological data collected by different laboratories using a common data

registration and database system is vital for these quantitative methods to gain momentum.

D. Databases

To be able to derive synaptic connectivity from static neuronal population data, we first need a representative sample of neurons which have been identified and mapped in 3D. More than 100 years of systematic mapping of a variety of structures and the morphological characterization of different neurons have amounted to a vast data source, which have been partially analyzed and the results published. Unfortunately, most of the original data are no longer available. It is now imperative to integrate independently generated data into one consistent database. The first problem is the data structure of choice to incorporate the full scale of complexity of static neuronal data. The language of the database must be vectorial to represent connections and flexible enough to accommodate new aspects. Born from this motivation, MorphML, a unified vectorial data structure has been designed for flexible representation of various neuromorphological objects from the subcellular level to the macroscopic scale morphology (http://www.morphml.org). The purpose of this data format is multifold. First, it enables incremental data integration across different laboratories and platforms. Second, it supports visualization of anatomical data as a rendering tool, designed specifically for this data format. Third, it provides a "core" data format that allows conversions between different morphological databases. Fourth, it supports the import of morphology data into dynamic modeling environments and simulation software such as Neuron (Hines and Carnevale, 1997) and Genesis (Bower and Beeman, 1998). Fifth, it could be maintained by industrial standard database management software (e.g., XML, IXL, Oracle). Currently, data conversion modules allow conversion of the Neurolucida data format to the 3D annotation system.

Arguably, it is now feasible to integrate different levels of morphological data and construct a detailed 3D representation of large population of neurons. With multiple-level data integration, it will soon be possible to reveal parts of the connectivity matrix by incremental development of the connectivity map based on morphological tracing. Furthermore, automatic data acquisition, either image analysis based or vectorial tracing, is expected to speed up data generation. Within the next 10 years, we anticipate that the complete 3D vectorial database of the rat brain will be available to address specific questions about hidden organization principles. A preliminary version of a database that allows integration and analysis of different 3D data sets collected at different levels and different laboratories that uses MorphML format can be viewed at http://www.ratbrain.org/ (Zaborszky *et al.*, 2005a). More details on this database and a list of other databases or electronic brain atlases can be found in the Appendix.

IV. DYNAMIC DATA

A. Dynamic System Approach

The inductive approach to understand network dynamics as a multiplication of single neuron operations fails for multiple reasons. First, inferences about the connectivity matrix, a prerequisite of functional connectivity, could not be made even with the complete neuromorphometric database. Recovering the connectivity matrix would require mapping all synapses onto each neuron, which is impractical. Secondly, given that all synaptic connections are mapped, calculating the range of dynamics exhibited by a connectivity matrix is intractable. Specifically, when trying to solve all the differential equations describing channel dynamics in multicompartmental models of a population of neurons, the effect of small uncertainties and the sensitivity for small perturbations scales with iterations so quickly that it could render the state of the neurons unpredictable.

Fortunately, it is not necessary to know all the connections and solve the differential equations for each compartment in order to predict the dynamics of a given network of neurons. There is a shortcut. Simulations on 20 million versions of a three-cell model of the pyloric network suggest that the number of possible different dynamics is much less than the possible synaptic strength configurations (Prinz *et al.*, 2004). Given the chance of reduction, theoretically we can classify circuitry architectures based on the invariant dynamics they generate. These dynamics at the mesoscopic[6] level may be robust enough to tolerate small differences in the subnetwork level organization (Freeman, 2000). Using this classification we can infer from the dynamics the architecture and vice versa. Recently, these dynamics became empirically permeable by using large-scale high-resolution recording of a population of neurons.

B. Large-Scale Recording of Neuronal Populations

1. Limitations and Constraints

To attain an empirical ground on large-scale network activity and capture the mesoscopic dynamics, we need to record as many neurons simultaneously as possible. Coincidentally, the number of neurons required to decode the location of a rat in an open space or the motion of the hand/arm on monkeys (both with better than 10-cm precision) is at least a hundred (Kemere *et al.*, 2004; Musallam *et al.*, 2004; Zhang *et al.*, 1998). To record this quantity of neurons at a single spike temporal precision is now feasible by extracellular recording. Imaging techniques are approaching this scale and

[6] An intermediate level between microscopic and macroscopic (Freeman, 2000).

will soon complement the extracellular recording methods. Albeit the spatiotemporal resolution of the blood oxygenation level-dependent signal and the indirect link between neural activity and hemodynamic changes make fMRI less suitable to capture the functional architecture on the cellular scale, recent advances in voltage-sensitive dye (Petterson, this volume) and two-photon calcium imaging (Goldberg *et al.*, this volume) are promising techniques to study the spatiotemporal dynamics of hundreds of neurons in the living brain. We focus on the extracellular recording technique in this chapter; however, the statistical approach for recovering functional connectivity from the spike pattern of multiple neurons is indifferent to the data acquisition technique.

Concerning the traditional extracellular recording technique, it is important to consider the limitation of the electrode. To date, the most commonly used electrodes are sharp electrodes, microwire electrodes, tetrodes, multiple wire electrodes, and electrode arrays. Positioning electrodes individually imposes a serious constraint on the number of electrodes. Practically, remote control operated individually movable electrode microdrives can control up to 16 electrodes. This may be sufficient to record activity of up to 30–40 neurons. To attain a simultaneous recording of > 100 neurons requires chronically implanted electrodes. Several configurations have been devised. One is an array of parallel microwires, mounted together allowing about 400 μm spacing between the 72 μm-diameter wires (MicroProbe Inc., MD). Another option is using silicon-substrate, micromachined probes that come in various shapes and configurations and cause much less tissue displacement relative to microwires. Among other configurations, multiple shank silicon probes allow simultaneous multisite data acquisition from the same cell as well as from the different cell groups (Vetter *et al.*, 2004). The third technology is the Utah electrode (the "Utah array"), which is a penetrating array of electrodes mounted on a 4 mm × 4 mm base containing 100 silicon spikes that are up to 1.5 mm long and designed to be implanted in primate and human cortical structures (Nordhausen *et al.*, 1996).

Another constraint in extracellular recording is sampling rate. To resolve spike shapes, the sampling rate must exceed 20 kHz per electrode. Sampling rates higher than 25 kHz do not improve spike discrimination significantly (Nadasdy *et al.*, 1998). A simultaneous recording of 100 channels at this sampling rate would require 2 MHz multiplexing with the digitized data streamed to a hard disk. If the signal is digitized at 16 bits per channel (12 bits is sufficient, 16 bits is recommended), then the necessary data transfer rate is 32 MB/s, which can be easily transferred in standard network cards and streamed to a hard disk. However, we still have to be cautious with disk space since 2 h of continuous recording with this bandwidth takes a total (nonredundant) disk space of about 28 GB per session.

Another important constraint is the type and geometry of the electrode. Multiplying electrodes can be done by bundling multiple microwires together. The standard technique is to bundle four electrodes to make a tetrode. This technique multiplies the recording sites around a single

neuron, improving spatial resolution and consequently spike discrimination (Buzsaki, 2004; Henze *et al.*, 2000). There is no substantial gain in neuron yield of bundling more than four microwires. Another way to increase the number of recording sites is by multiplying electrode arrays that are mounted separately. Several such electrode configurations have been deployed through the last 15 years. There are two basic strategies, concerning the type of scientific questions addressed. One strategy is to chronically implant as many electrodes as possible, where it is certain that a number of electrodes will not detect any signal from active neurons, simply because they cannot be individually positioned near the neurons. The alternative strategy is to make the individual electrodes independently movable. This technique is better suited for acute preparations where the research objective requires inserting electrodes in different locations every day for systematic mapping. Chronically implanted tetrodes are between these two strategies since the whole tetrode array can manually be lowered every day. Electrode configurations for chronic implants range from 16 (MicroProbe Inc., MD) to 100 (Utah probe, University of Utah, Salt Lake City, UT) recording sites, on a single connector. Many laboratories use custom-made electrode arrays. Electrode implants can be skull mounted or floating. To minimize movement artifacts, it is critical to keep the electrode and signal stable. The stability of floating electrodes is higher than that of skull mounted because the electrode moves with the brain.

Extracellular recording strategies have to consider several trade offs. In order to increase the neuronal yield of recordings, the obvious strategy is to multiply electrodes. However, the cost of multiplying electrodes is multifold. First, the tissue displacement increases with the number of electrodes. According to simulations, a vertically inserted 50-μm-diameter microwire electrode collides with 80% of the dendrites of the nearest recorded neuron (Claverol and Nadasdy, 2004). Second, the increased number of channels requires upgrading the data acquisition hardware to keep the sampling rate at least 20 kHz per channel and stream larger data blocks to a hard disk. The third factor is that the isolation of neurons from an increased number of channels substantially increases the volume and time of data processing. For example, a thorough manual spike sorting of a 2-h recording from eight channels may take 2 weeks in our practice. Considering that for publication it is necessary to process at least 30 such recordings and to replicate it at least on one other preparation, it would take more than 2 years of graduate student life with no weekends off to publish. Consequently, 100 channels would take at least 28 years to analyze which may eventually delay graduation.

2. Signal-Based Source Identification

A typical microwire electrode or tetrode can detect signals from neurons as far as 150 μm away (Fig. 20.6). Such a volume contains about 1100 neurons based on hippocampal cell density estimates (Henze *et al.*, 2000). The probability of detecting neurons decreases with the distance from the electrode. In the outer part of this volume no individual spikes are discernible primarily

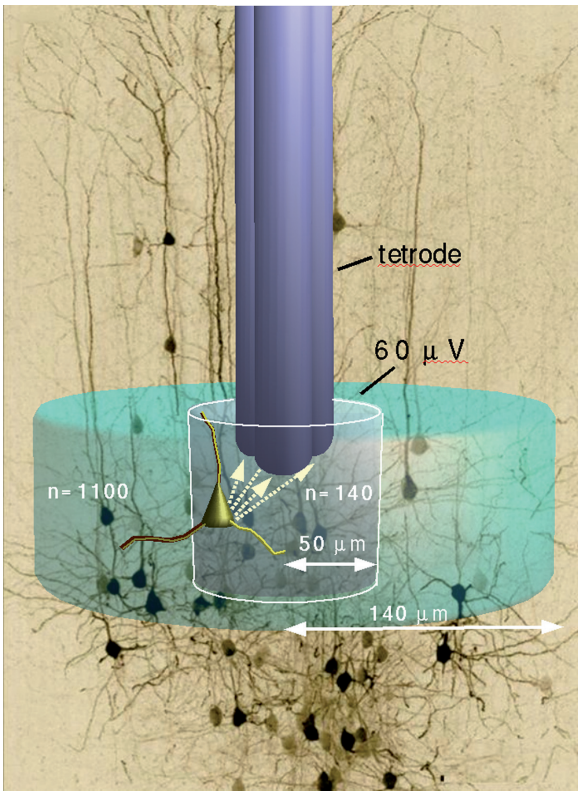

Figure 20.6. The simplified scheme of single-unit isolation from extracellular recording. The montage is an artistic rendering of a ∼300-µm-wide cortical volume with the tip of a ∼50-µm-diameter tetrode inserted in the vicinity of pyramidal cells. The broad blue cylinder represents the largest distance from the electrode within which spikes can be detected. This volume contains ∼1100 neurons. The 50-µm-radius inner cylinder is the volume within which spikes are discernible. A pyramidal cell (highlighted) at the vicinity of the electrode projects differential signals to the four electrode tips as a function of distance. Since the voltage attenuates proportionally with the distance, the location of the source can be recovered from the differential amplitudes reaching the electrodes. Although this volume contains ∼140 neurons, one can usually record up to 8 neurons. In the volume around the 50 µm radius, the signal amplitude drops below 60 mV. From this point we can consider the signal "multiunit," where individual spikes are still detectable but cannot be identified with discrete sources. From this range to the 140-µm range, the signal asymptotically converges to noise as spikes from an increasing number of neurons start to overlap. Numbers are based on hippocampal estimates (Henze *et al.*, 2000). (Background image is enhanced GFP-expressing lentivirus injected into the parenchyma of rat layer 2/3 somatosensory cortex from Brecht *et al.*, 2004.)

because spikes at average firing rate overlap in time and space, making the signal similar to $1/f$ type noise. Within the inner volume of 100 µm, spikes become discernible; however, due to the additive background noise, the amplitude variation is too large to classify neurons. It is only within a 50-µm radius volume around the electrode that spikes can reliably be associated

with neurons. Intriguingly, based on a hippocampal cell density estimate, ~140 neurons should be detectable from this volume, we typically discriminate only a small fraction, on average less than 10 neurons. Whether this discrepancy is due to the silence of neurons or other attenuating factors, remains to be clarified.

In order to associate spikes with neurons, most spike-sorting methods use waveform-discrimination-based algorithms. The underlying assumption behind this group of methods is that the spike waveform differences correspond to different neurons. The biological justification for this assumption is the point source model of action potential generation. According to this model, action potentials going down the axon of the same neuron are almost identical if you measure it near the axon hillock or intracellularly from the soma. Consequently, the main source of variation of mixed waveforms is the distinct spatial location of the neurons relative to the electrode. However, the point source is affected by a number of other factors that need to be considered. For example, the intrinsic dynamics of spike generation (the interaction of back-propagating action potentials and dendritic spikes), the cell type (interneuron versus pyramidal cell), and ongoing local field oscillations substantially contribute to the spike waveforms (Buzsaki *et al.*, 1996) either by moving the point source or by adding a nonlocalized variance to the waveform.

An alternative approach in spike sorting is based on the spatial localization of the source. This principle was first utilized by the stereotrodes and further exploited by the tetrodes. Projecting simultaneous traces of spike waveforms (all data points or only peak-to-peak values), measured from two adjacent electrodes as X and Y coordinates against each other, results in clusters of points. These clusters reflect the differential amplitude ratios caused by the unequal distance of the neurons relative to the two electrodes. Using multiple recording sites within the critical 50–60 μm volume and knowing the spacing between the sites, one can triangulate the sources (Nadasdy *et al.*, 1998). Sources determined from the amplitude ratios of collinearly arranged recording sites discriminate between neurons more reliably than spike waveforms (Harris *et al.*, 2000). Silicon multiprobes further expand the "scope" of electrodes. For example, multiple shanks and collinearly arranged recording site geometry with 20 μm spacing provide precise localization of neurons as well as reliable segregation of different groups of neurons from each shank (Csicsvari *et al.*, 2003). The distance and geometry of recording sites can be optimized for a given structure of interest.

3. Spike Sorting

While electrodes and amplifiers allow recording from more than 100 channels simultaneously, isolation of single units from all of these channels is one of the main bottlenecks of data processing. Spike sorting is a critical step not only for isolating the sources of spike generation but also for classifying neurons. More research is needed to elucidate the relationship between

action potential generation and current propagation in the extracellular space in order to maximize information available from the waveforms. For example, it has been reported that spikes generated by interneurons have a shorter polarity reversal (spike half width) than do pyramidal cells (Bartho *et al.*, 2004). The correlative inference from the average spike shape to the type of neuron can serve only as a putative classification considering that the waveform can be affected by many other factors. Combining evidences including firing rate statistics and cross-correlation analysis is necessary to classify neurons based on dynamic properties.

Spike-sorting methods consist of two main steps: feature extraction and clustering. The goal of feature extraction is to determine a set of discriminative features which, when projected to an n-dimensional space, best separate individual spikes. When spikes are classified based on waveforms, either the whole spike shape or several descriptive features are used (Abeles and Goldstein, 1977; Fee *et al.*, 1996, respectively, and review by Lewicki, 1998). In either case, the database usually contains redundant dimensions that are suboptimal for clustering. The most common method to reduce dimensionality of spike features is based on the principal component analysis (PCA). Using PCA, the main axes of "ideal" projection are determined by the largest two eigenvalues (Abeles and Goldstein, 1977). Although the largest eigenvalue projections maximize the global variance of the whole spike sample, they may not be optimal to separate the clusters. A more recent approach is based on clustering wavelet coefficients computed from the individual waveforms (Quian-Quiroga *et al.*, 2004).

It has been argued that the main causes of unit identification errors regardless of the method being used are (1) the additive noise derived from overlapping background activity, (2) the intrinsic amplitude modulation of the spikes due to subthreshold membrane oscillations, (3) somatodendritic back propagation of action potentials (Buzsaki, 2004), and (4) the human operator's ability to supervise the clustering (Harris *et al.*, 2000). The human operator's suboptimal performance and the time constraint are the main motivations to develop quasi or fully automatic and unsupervised spike-sorting tools. As the number of electrodes and channels increases, isolation of single units (spikes generated by a distinct neuron) "online" during the experiment simply cannot be performed reliably by a human operator. Such unsupervised spike-sorting methods have already been deployed (KlustaKwik, http://klustakwik.sourceforge.net/; WaveClus, Quian-Quiroga *et al.*, 2004). For a while, off-line spike sorting will remain necessary simply because the online classification is CPU intensive and requires more time to classify a channel than to record from it.

C. Reconstruction of Functional Connectivity

Spike sorting identifies spikes with a distinct neuron, thus allowing the reconstruction of multiple spike trains. The next major step is to recover

the hidden functional architecture of these neurons, based on the temporal correlation between the spikes in different spike trains. Before this step is taken, we need to distinguish between sources of temporal correlations. Correlations in neuronal activity can be caused by the spatiotemporal structure of stimuli or can be derived from the functional connectivity of neurons.[7] The former one is referred as signal correlation and the latter one is referred as noise correlation. Usually both sources contribute to the actual activity pattern. To elucidate the functional connectivity, we must consider the intrinsic variance in neuronal activity, i.e., the variance that is independent of the input signal characteristics. Therefore, the input to the studied circuitry should either be kept constant or assumed to be evenly distributed. If each neuron is an ideal encoder, which encodes the stimulus independent of other neurons, then all correlations can be explained by the stimulus and there is no circuitry to uncover. In contrast, the typical scenario is that the input can only be partially recovered from the activity of neurons, suggesting that a nontrivial circuitry is involved where neurons are not independent. The answer for the general question "whether neurons encode the input independently from one another or not" likely depends on the studied structure. The complexity of dependence greatly affects the level of statistics efficient to recover the circuitry from the activity of neurons.

If neurons are highly interdependent, then recovering the circuitry is a complex and computationally NP-complete problem* where the computation time is an exponential function of the number of cells (spike trains). Therefore, the first practical step is to reduce the complexity to pairwise cross-correlations of spike processes and build the functional connectivity from the pairwise relationships. Several cross-correlational techniques have been developed, primarily between spike trains of two neurons. Nonetheless, higher order correlations are also practical to compute.

The first-order relationship between two spike trains is captured by the cross-correlation and cross-coherence of the two spike trains. For the calculation of the cross-correlation function see the Appendix. The graphical representation of cross-correlation is the cross-correlogram. The qualitative evaluation of cross-correlogram can tell (i) the independence of the two spike generation processes, (ii) the time precedence between the two processes, and (iii) the polarity of the effect (inhibitory/excitatory). What a cross-correlogram does not determine is whether the dependency between the two neurons is direct or indirect. The interpretation of cross-correlograms is illustrated in Fig. 20.7. Cross-correlograms are constructed by treating one spike train as the reference and the other train as the

[7] The method of reconstructing the stimulus from the activity is called the reverse correlation technique.

*NP-complete problems are decision problems verifiable in non-deterministic polynomial time.

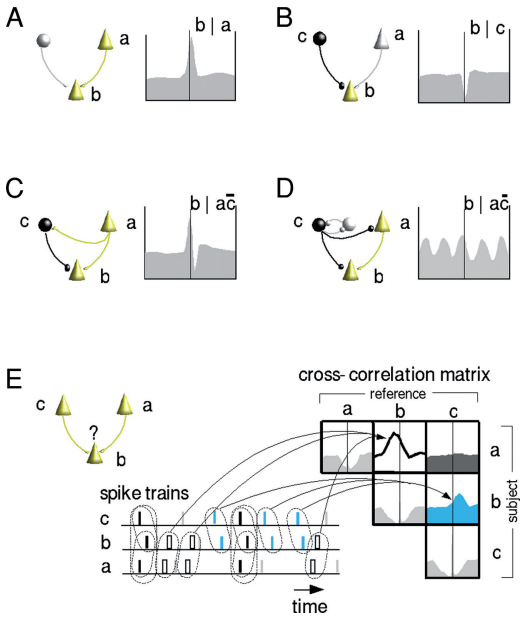

Figure 20.7. Inference from cross-correlations to circuitries. (A) A central peak with a few millisecond delay indicates a monosynaptic excitatory drive from neuron *a* to *b*. (B) A central through is suggestive of a monosynaptic inhibitory drive from *c* to *b*. (C) A central bipolar wave with positive peak followed by the through indicate a feed-forward excitatory drive (*a*–*b*), followed by recurrent inhibition (*a*–*c*–*b*). The opposite polarity order would suggest feed-forward inhibition combined with a non-monosynaptic recurrent excitation (not shown). (D) Periodicity in the cross-correlogram is consistent with an excitatory drive from *a* to *b*, modulated by an oscillatory input from a locally phase-coupled interneuron circuitry *c*. Alternatively, the same cross-correlogram can reflect two inhibitory interneurons firing in synchrony (not shown). (E) A fictitious example for a three-neuronal excitatory circuitry illustrates the limitation of cross-correlation analysis. Neurons *a* and *c* both terminate on *b*. It is evident from the cross-correlogram that *a* drives *b* with certain delay (represented by outlined area in the cross-correlational matrix and corresponding empty ticks in the spike train inset). The *c*–*b* cross-correlogram also indicates an excitatory drive between neurons *c* and *b* (blue area and blue ticks in the spike train inset). However, the flat *a*–*c* cross-correlogram suggests that spikes of neurons *a* and *c* coincide only by chance (gray area in the cross-correlogram). The dilemma, whether *a*–*b* and *c*–*b* drives are conjunctive or disjunctive, i.e., *a* and *c* drive must coincide to excite *b* or any of them is sufficient to drive *b*, cannot be resolved based solely on the pairwise cross-correlograms. One needs to look at the triple cross-correlogram and evaluate whether the frequency of $a - b - c$ triplets (indicated by black ticks in the spike train inset) is higher than chance or not. (This panel is modified from Nadasdy, 2000).

subject. The computational algorithm of the cross-correlogram goes as follows:

1. Define a time window *W* of interest. This is usually longer than the refractory period (3 ms) and smaller than the longest causal interactions

within a network (200 ms). Moreover, define a Δt precision of spike time measurement. Reasonably, this should be larger than the spike width and smaller than the expected smallest spike time precision, but not larger than $W/20$.

2. Then iteratively, take the next/first spike at the reference train and look for spike coincidences on the subject train within the time window centered around the reference spike. The time lag τ (see the Appendix) of the subject spike train can either be negative when preceding or be positive when following the reference.
3. Next, the bin of the cross-correlation histogram at τ is incremented.
4. After all subject spikes within W have been registered, move the time window to the next reference spike and repeat steps 2–3 until the last spike has been used as the reference spike.

The interpretation of cross-correlations is summarized in Fig. 20.7. The objective of cross-correlational analysis is to determine the interaction between two neurons (reference and subject neurons). Since correlation can occur due to a causal effect by one neuron on the other neuron, as well as due to a causal effect by an outside source on either of the two neurons, the reduced model of interactions must include at least three neurons. When considering the dynamics of a three neuronal (a, b, c) subnetwork based on the information available from two neurons, the possible cross-correlations are consistent with one of the following schemes: (i) excitatory drive from a to b (Fig. 20.7A); (ii) inhibitory drive from c to b (Fig. 20.7B); (iii) combined excitatory and inhibitory drives (Fig. 20.7C); and (iv) common oscillatory drive to a and b is also evident from cross-correlograms (Fig. 20.7D).

D. Effective Connectivity

Although action potentials are uniform in shape and generation site, the inputs that elicit them derive from many neurons firing at different times. In principle, a strong input connection has a larger contribution to a spike series than a weak input. In order to recover the functional connectivity between neurons from an extracellular recording, it is important to determine the most effective source of input for a given neuron. The tight temporal correlation between the input and the output spikes is the key to resolving which spike was caused by which neuron in the network, even when higher order (hidden) dependencies are involved.

Higher order dependencies, involving three or more neurons, are beyond the scope of the cross-correlation method. Consider the example illustrated by Fig. 20.7E. Let us assume that we know the connectivity between the three neurons (a, b, c), where neuron a and c both have an excitatory drive on neuron b. The excitatory dependencies between a–b and c–b are evident from the combined cross-correlograms (on the right). Nonetheless, we would like to know whether a single input from neuron a or c is sufficient

to excite b or the two inputs must coincide to excite neuron b.[8] From pairwise cross-correlations this information is not available. To infer the "effective connectivity" from multiple spike trains involving more than two neurons requires higher order statistics.

Motivated by mapping the "effective connectivity," Gerstein and colleagues introduced the joint peristimulus time histogram (JPSTH) method (Aertsen *et al.*, 1989). The JPSTH was a generalization of cross-correlation method to spike triplets of different neurons that coincide within the time window W. The appropriate statistics were developed much later (Abeles and Gat, 2001; Baker *et al.*, 2001; Frostig *et al.*, 1990; Palm *et al.*, 1988). As an illustration of such statistical analysis on >2D dependency between spike trains, consider Fig. 20.7E again. The joint occurrence of an *abc* triplet is simplified by reducing it to the coincidences of two intervals, τ_{ab} and τ_{ac} interspike intervals. In a random spike process, we assume that the *acb* triplets are merely by-chance co-occurrences of the *ab* and *ac* intervals. Therefore, their joint probability is the product of the component probabilities. Otherwise, the triplets are not random coincidences:

$$H_0\colon P_{acb} = P\tau_{ab} \cdot P\tau_{ac}$$
$$H_A\colon P_{acb} \neq P\tau_{ab} \cdot P\tau_{ac}$$

If it turns out that $P_{acb} > (P\tau_{ab} \times P\tau_{ac})$, that is, the observed frequency of the triplet is higher than the product of the individual probabilities, then the *acb* triplets must be coordinated above chance coincidence of *ab* and *ac* intervals. The $P\tau_{ab}$ and $P\tau_{ac}$ probabilities are estimated from the pairwise cross-correlation functions; however, the two interspike-interval pools are not mutually exclusive because they both contain a fraction of the other interval pool. For example, the *ab* cross-correlations include the *abc* events and likewise the *ac* cross-correlations, consequently these events will be counted twice. As a result, the product of cross-correlation functions overestimates the expected probability of triplets. Therefore, the product must be corrected and renormalized to fit to the individual firing rates and cross-correlograms. This renormalization must conform not only with the $P\tau_{ab}P\tau_{ac}$ cross-correlations but also with the $P\tau_{bc}$. Because the true probability density functions are not directly available from the data, various computational methods have been developed for estimating it. The correct estimation of random coincidence is critical in order to determine the confidence interval for significance testing. Among those methods, we point the reader's attention to the method of calculating a "surprise function" (Palm *et al.*, 1988), spike jittering or "histogram blurring" technique (Abeles and Gat, 2001) and time resolved cross-correlation method (Baker *et al.*, 2001).

[8] Although there may be thousands of excitatory inputs terminating on a pyramidal cell, the above question, whether the two cells (a, c) belong to populations that have a conjunctive or disjunctive effect on neuron b, remains relevant.

An alternative approach to detecting hidden dependency time structures from spike trains is based on searching for joint events using pattern-searching algorithms. The rationale behind this approach is the following. When several neurons are recorded simultaneously, these neurons are part of a larger hidden network. We further assume that neurons are finite state machines and spikes are generated from neuron to neuron as a *causal sequence* of state transitions. If a sequence occurs more often than chance, we have a statistical basis to believe that the spike sequence follows a deterministic process, which is constrained by the network architecture (unless it was imposed by the temporal structure of the input to the structure which we do not consider here). If the circuitry favors one spike sequence over other sequences, then this sequence must recur more often than others. Consequently, the most invariant sequence must be related to the activity flow, which in turn, is dependent upon the circuitry. Thus, the objective of pattern searching spike trains is to determine repeating sequences and reconstruct their underlying functional connectivity. Various algorithms of searching the high dimensionality space of multiple spike trains for repeating motifs of spikes were introduced during the last 10 years (Abeles and Gerstein 1988; Nadasdy *et al.*, 1999; Lee and Wilson, 2002; Ikegaya *et al.*, 2004). The common feature of these algorithms is to define a template motif $S_j = \{t_j^{j1}, t_{j+1}^{j2}, t_{j+2}^{j3}, t_l^{nm}\}$ from the data, which is a vector of spike latency t of the ith spike generated by the jth neuron where j = [1 . . . n]. Let us name this as an n sequence. Then the computer program performs iterative searches by comparing the template n sequence with each instance of n sequences on a data segment where the length of n sequence is equal to the dimension of searching space n. After every partial match between the template and the data, the dimension is incremented until n. When the search is complete for a given template, the template is replaced by a new n sequence from the data and the searching session starts over. After an exhaustive search of the whole database for all possible S_i sequences, the detected recurring n sequences can be rank ordered and those that occur more than chance are considered to be representing the predominant flow of activity within the network of the given set of neurons. As we have mentioned, the searching process is CPU intensive and computation time increases exponentially with the number of spike trains. A spike train database of 100 neurons would require a supercomputer to run the search.

Since dependency and causality are interchangeable terms, reconstruction of effective connectivity from dynamic data can be approached as recovering the hidden causal sequence of activity flow within the network. The formal definition of causality on time series was first introduced by Granger (1969) in the context of linear regression models of stochastic processes and since then it is referred as "Granger causality." Accordingly, if the variance of the prediction error from a time series $Y(t)$ is reduced by including the past measurements from time series $X(t)$, then the time series $X(t)$ "caused" the time series $Y(t)$. Independent of the Granger causality, numerous other attempts were made to quantify causality from neuronal data. To take a

full advantage of multichannel data, such as simultaneously recorded spike trains, Kaminsky and Blinowska (1991) suggested a multivariate spectral measure to determine directional influence, defined as the "directed transfer function," which is fully compatible with Granger causality (Kaminsky *et al.*, 2001). Using the formalism of directed transfer functions, one can reconstruct the causal-dependency network within a population of neurons. It is important to note that Granger causality does not imply direct causal effect between the two spike trains (i.e., neurons). The effect can be mediated by other (hidden) neurons or distributed over the whole population of neurons, which would make the causal sequence untraceable. However, the question of direct causality can also be addressed within the framework of directed transfer functions (Kaminski *et al.*, 2001). Granger causality spectra have been successfully applied on local field potentials, clarifying interactions between different recording sites at specific frequency bands, (Brovelly *et al.*, 2003) and can be applied to point process spectra such as spike trains (Kaminski *et al.*, 2001).

A problem common in all these methods is the definition of confidence. To obtain confidence intervals for significance estimations, we need to know the probability density function of the given variable, such as triplet occurrence, sequence repetition, or causality. Since there is no a priori knowledge about the generative process of these variables, we must rely on Monte Carlo methods, such as the simulation of the spike generation process and the construction of surrogate spike trains (Nadasdy *et al.*, 1999). The limitation of the Monte Carlo approach is that we can never be sure that randomization of a variable leads to a biologically plausible null hypothesis or not. Consensus on these methods has yet to be achieved.

In summary, to recover the functional connectivity from a local cell assembly based on the dynamics, the following methods should be applied. Use electrodes with multiple recording sites at 20–50 μm apart allowing multiple spike measurements from the same neuron. Combining several such electrodes with at least 100–200 μm spacing between them allows the recording of nonoverlapping groups of cells. Configurable recording geometry is preferred to suit the electrode to the size and cytoarchitecture of the target tissue. For an optimal design, the potential tissue displacement and interference with normal neuronal functions should be considered. Using an unsupervised spike-sorting software, the classification of 3–7 neurons from a single electrode (shank or tetrode) is feasible, which scales up with the number of electrodes used. Cross-correlations can be applied to reveal first-order dependencies. Higher order statistics, essential for reconstructing the network dynamics, can be computed by joint probability and sequence-searching algorithms.

An example of the complete process of the reconstruction of effective connectivity is shown in Fig. 20.8. Cortical recording from the somatosensory cortex of an awake rat was performed by using a silicon microprobe (Buzsaki, 2004). For illustration purposes, the image of the electrodes was superimposed on the histological section using electrode traces as landmarks.

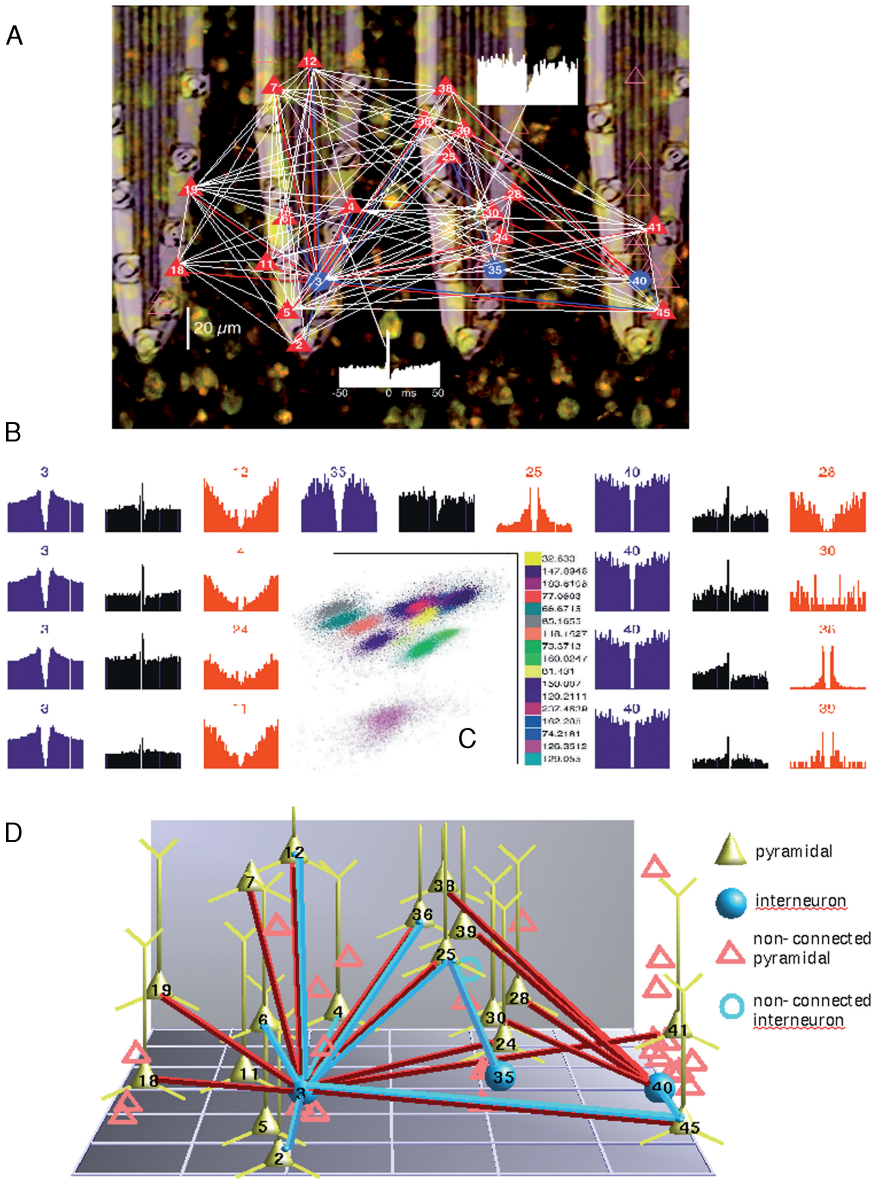

Figure 20.8. Reconstruction of effective connectivity between neurons based on the temporal coherence of spiking activity recorded extracellularly from the somatosensory cortex of a rat. (A) The theoretically possible network of neurons is illustrated by white lines (only a subset) connecting putative pyramidal (red triangles) and interneurons (blue circles). Neurons were isolated using spike sorting and localized by calculating the "center of mass" of the spike amplitudes. The putative locations enabled identification of neurons with their histological traces (background) and recovery of the electrode traces. The image of the multiple shank silicon electrode was aligned and superimposed on the traces. Spacing between adjacent recording sites of the electrode was 20 μm with 200 μm intershank distance (electrode shanks

The neurons isolated from each electrode were localized by calculating the center of mass of their spike amplitude. Possible functional connections were considered by pairing all these neurons and computing pairwise cross-correlograms of their spike times. Neurons with the largest modulation were selected as active nodes of the functional network, using the cross-correlation function. Interneurons and pyramidal cells were identified based on their firing rate and the polarity of the cross-correlation modulation. Reciprocal connections were also evident from the cross-correlograms. Note that not all of the recorded neurons are engaged in the network. The fact that certain neurons did not participate in the functional network supports the validity of detected connections. Using such heuristics, one can construct a network that is most consistent with the dynamics sampled by the cross-correlations. Although this network is rather incomplete and connections are only putative, it is the most reliable method to date for parsing the architecture of circuitries.

V. CONCLUDING REMARKS

After a century of extensive piece-by-piece brain mapping, finally all the main pathways of the central nervous system have been described and validated across different species. Although for most structures the cytoarchitecture has been defined and major cell types have been identified, the key principles that relate the microscopic architecture to activity patterns are still unknown. We argue that the conceptual bridge between these two levels is the dynamics of microcircuitries. The microcircuitry is a mesoscopic entity between neurons and macroscopic networks that generates a dynamic mosaic of functional cell assemblies by assigning neurons to different subnetworks, and these subnetworks are dynamically allocated to various functions. We reviewed classification of these microcircuitries as precursors for "basic circuitries." Although the catalog of basic circuitries is at the doorstep, to be able to make inferences from the architecture to the activity pattern and vice versa requires a coordinated anatomical and physiological approach that embraces both static and dynamic aspects of neuronal data acquisition.

←

Figure 20.8. (*Cont.*) were brought closer for illustration purpose). (B) Auto- and cross-correlation histograms featuring the coherency between the three interneurons (numbers 3, 35, and 40). The autocorrelograms for interneurons are purple, interneuron–pyramidal cell cross-correlograms are black, and pyramidal cell autocorrelograms are red. (C) The main PCA clusters show clear isolation of single units. Numbers at the right are the Mahalanobis distances for the given cluster. (D) Effective connections verified by the cross-correlational analysis among the theoretically possible network. Neurons whose connectedness could not be verified are marked by empty symbols. Note that most pyramidal cells receive inhibitory connections from the interneurons. A few of these connections are reciprocal. In contrast, no pyramidal–pyramidal connection was observed.

Basic circuitries are recognized as instrumental for filtering and generating specific activity patterns and oscillations. Their cellular composition must be specific for the given structures and consistent across different species. Plausibly, the evolving and developing brain multiplies these circuitries as basic information-processing units to construct large networks. The unique features of basic circuitries are the constituent neuron types, connections, and the specific activity patterns they implement. We argued that these activity patterns cannot be derived from the physiology of isolated neurons. Instead, the focus needs to shift from single-cell recording to the circuitry of ensembles of neurons, an approach that involves a combination of neuroanatomical and physiological methods.

Among these methods, this chapter discussed algorithms designed to extract information from a large population of neurons that is relevant for functional considerations, such as neuronal clusters. We also reviewed methods of collecting physiological data that capture the dynamic aspects of circuitry function, such as spike pattern generation. We highlighted on methods of the multiple electrode recordings and the analysis of action potential patterns generated by a population of neurons. We illustrated the inferential processes from the two opposite directions: one that proceeds from the structure to the dynamics and the other that proceeds from the dynamics to the structure. The two types of inferences complement each other and they should converge to a solution where the circuitry architecture is consistent with the activity pattern. The circuitry and activity pattern as a functional unit may be considered as a fundamental building block of the nervous system.

Concerning strategies of neuronal tract-tracing methods, two dominating tendencies, the expanding computational approach in neuroanatomical data analysis and combining existing methods, are broadly covered by different chapters of this volume. Specifically, using a sophisticated combination of tracing methods, the synaptology of any circuitry can be accurately determined (Sesack *et al.*, this volume). Using extracellular, juxtacellular, and intracellular recording methods (Duque and Zaborszky and Sik, this volume), the anatomical features can be correlated with an electroencephalogram, multiunit activity, local field potential, and intrinsic membrane characteristics. Functional networks or entire brain regions are available for reconstruction (Bjaalie and Leergard, this volume) and statistical methods on testing structural hypotheses have already been developed (Bjaalie and Leergard, this volume). Furthermore, neural functions can be correlated with microstructural variation (Amunts and Zilles, this volume).

Last but not least, we emphasized the importance of 3D representation and the use of volumetric data structure that is a prerequisite for exploiting the information available from neuronal tracings. The third dimension is critical to complete the paradigm shift we are witnessing in three major fronts of research: (i) functional neuroimaging, (ii) computational data analysis and visualization, and (iii) data sharing and integration into incremental databases.

APPENDIX

A. Parametric Modeling of Neuroanatomical Data

1. Definition of Volumetric Database

A volumetric database consists of a 3D distribution of one or more variables. For the sake of simplicity, let us focus only on one variable. This variable must have spatial gradients that are continuous in space. Usually this variable is the density of a given feature. Therefore, the first step of constructing a volumetric database is to define this structural feature (such as the cell body, the dendritic segment, or the expression of certain marker), which has spatial density gradients. Before extracting this variable the space needs to be discretized. Discretization is generally achieved by defining a grid structure that is optimal for sampling the data. Reasonably, the grid size must be large enough to contain multiple instances of the given feature, but small enough to represent the fine-scale spatial variation of the variable. We refer to the 3D units of the grid as voxels. The voxel size determines the spatial resolution of the density of the variable. Voxels can also be considered as 3D bins within which the instances of the variable are counted. The voxels usually, but not necessarily, have equal edge lengths and each voxel is addressed by its Cartesian coordinates (x, y, and z).

2. Construction of Volumetric Data of Neuronal Density

The given camera lucida database (we recommend Neurolucida, however, it can be another 3D vectorial data type) must be exported as an ASCII file and parsed for cell bodies and structure outline coordinates. As a result, the data should contain only cell bodies $\{b_t\}$ of a given cell type t, represented individually by their single Cartesian point coordinates $\{p_{xyz}\}$ and section identifiers s. If the z coordinates were not recorded, the section identifier should be considered as the z coordinate.

$$b_t = p_{xyz} \tag{20.1}$$

Conversely, since a given position could be occupied by only one cell body, the Cartesian coordinates together with the cell type completely define a cell b_t as x_b, y_b, z_b, and t. Structure outlines can be compiled to separate files. The medial, lateral, dorsal, and ventral extremes of the cell population should be taken as edges of a 3D framework to incorporate the region of interest. The total volume V occupied by neurons (neuronal space) is expressed as a vector $\vec{r}$ with minimal r density function:

$$V = \{\vec{r} : \rho_{\vec{r}} > 0\} \tag{20.2}$$

For quantitization of local density differences, V was subdivided into "voxels" and defined as follows:

$$v = d_x, d_y, d_z, \tag{20.3}$$

where d is the edge of the voxel. If the within section depth of the coordinates were not registered, the section index s can be used as d_z. Thus, voxel and cell definitions can be simplified as $vs = d_x$, d_y and $b_i = p_{xys}$, respectively. The i, j, and k indices of a voxel containing a $b_i = p_{xys}$ cell body is calculated as

$$i = d_x \left(\frac{x_p}{V_{\text{length}}} \right), \quad j = d_y \left(\frac{y_p}{V_{\text{width}}} \right), \quad k = s. \tag{20.4}$$

Cells are then counted in each voxel for each cell type separately, providing a local density function ρ:

$$\rho_{(v_{ijk})} = \text{count}\,(v_{ijk}) = nb_i. \tag{20.5}$$

For visualization, we define a volume Ω based on a function of minimum density σ:

$$\Omega = \left\{ v_{ijk} : \rho_{(v_{ijk})} \geq \sigma \right\}. \tag{20.6}$$

The anatomical distribution of high-density locations is often visualized by a manifold rendered around the volume and denoted as $\delta\Omega$. The manifold can be defined by surface rendering and carried out using commercially available visualization tools such as the Matlab software package (MathWorks, Natick, MA). After surface rendering, one must pay attention to convert the voxel coordinates back to stereotaxic coordinates or coordinates used by the data acquisition system to be able to superimpose the voxels on structure outlines.

Note that the critical step was the conversion of the 3D point-coordinate database, where the entries were the cells, to density data (Eq. 20.5), which became a volumetric database. In contrast to the original parametric database where cell bodies are represented by their x, y, and z coordinates, the entries of the volumetric database are cell density or cell count. The key advantage of the volumetric database is that it allows one to employ parametric statistical methods. Moreover, it enables one to slice data at any angle and visualize it from any point of view.

3. Differential Density 3D Scatter Plot

Valuable information can be extracted from the volumetric database that is not available from the 3D tracings of cells. To extract structural features and visualize them, we use the example of cell density. The density of neurons is indirectly related to functional clusters of the population because neurons close to one another are likely sharing input. We can apply a density threshold and highlight voxels with higher than threshold density. Taking the visualization one step further, we randomly choose a neuron from the selected voxels and visualize that neuron superimposed on the background of local density. Furthermore, we can select not only one but n number of neurons from a given voxel, where n is proportional to the density.

4. Isodensity Surface Rendering

The spatial organization of a large population of neurons can be very complex. Instead of visualizing each neuron, the global pattern of density differences may elucidate important structural principles that are not apparent from a large population of neurons. Surface rendering around high-density cell groups can capture this global pattern. We developed an algorithm that renders a surface around voxels where cell density is larger than a certain threshold. The procedure of discretization of the 3D space into voxels and calculating the per voxel cell density is described under section "Construction of Volumetric Data of Neuronal Densities." By applying different density thresholds, the sharp transition of neuronal density captured by two thresholds can be indicative of the size of a neuronal aggregate. The stepwise increase in density may be related to deviation of randomness that requires further statistical tests.

5. Isorelational Surface Rendering

In order to simplify the complex spatial relationship of large neuron populations and extract the associative relationship of different cell types, we can calculate the density ratio of the two cell types in each voxel. Highlighting the locations at which the density ratio exceeds a certain level reveals the spatial configuration of the cell-to-cell associations between different cell types. To illustrate this, first we constructed volumetric databases of density for each cell type and discretized the space by dividing it into voxels. For this, the different cell types must be carefully mapped to a common 3D coordinate system. If the different cell types were traced from different sections, it must be considered that inference of the joint density from separated sections may be affected by section distortion. If density changes between adjacent sections are negligible, the within-section z coordinates of different cell types can be collapsed into the same section s to obtain an estimate for the real joint density. The next step is to calculate local density ratios between the cell types for each voxel. When density ratios had been assigned to each voxel of the volumetric database, we imposed a predefined density ratio criterion and selected voxels that met this criterion for visualization. The volume of these voxels represented a specific numerical association between cell types. Voxels where the predefined density ratio of cell types had been established were surface rendered. Thus, cell bodies with density ratios larger than a specific value were covered by the surface. Conversely, voxels with density ratios smaller than the critical one were located outside of the surface. The unique feature of the "isorelational surface rendering" method is the visual representation of an abstract relationship that may be more important for understanding the functional architecture of neurons than the exact locations of cell bodies. For visualization purposes, a range of critical density values must be applied for testing the integrity of clouds and

to make sure that there are no hollow spaces covered. Examples for analyses described under sections "Differential Density 3D Scatter Plot," "Isodensity Surface Rendering," and "Isorelational Surface Rendering" can be found in Nadasdy and Zaborszky (2001) and Zaborszky *et al.* (2005b).

B. Databases

1. List of Electronic Databases of Rodent Brains

Brain Maps	Swanson	Computer Graphic Files, Elsevier, 1992–1998
3D Rat Brain	Timsari *et al.* (1999)	http://www-hbp.usc.edu/Projects/3dAtlas.htm
The Rat Brain	Paxinos and Watson	Academic Press, 1998–2005 CD-ROM
Brain Browser	Bloom and Young	Academic Press, 1993
Rat Brain	Toga *et al.* (1995)	www.loni.ucla.edu/Research/Atlases/Rat/Atlas.html
Rat Brain	Nissanov and Bertrand (1998)	www.neuroterrain.org
IMGEM Mouse Brain	Sugaya *et al.*	http://sugaya.ucf.edu
Mouse Brain	Allen Project	www.brain-map.org
Mouse Brain Library	Reed *et al.* (1999)	www.mbl.org/mbl_main/atlas.html
Comp Mouse Brains	Hof *et al.*	http://www.neuroscion.com/laboratory/mousebrainmaps.html
Brain for Macintosh	Nissanov, Tretiak	http://ece.drexel.edu/ICVC
Mouse Atlas Project	Baldock *et al.*	http://genex.hgu.mrc.ac.uk
Rat-Brain Atlas	Pich, Danckaert	http://www.gwer.ch/qv/ratatlas/ratatlas.htm
Mouse MRI Images	Jacobs *et al.*	http://www.gg.caltech.edu/hbp/atlas.html
High-Resolution Mouse Atlas	Sidman *et al.*	http://www.hms.harvard.edu/research/brain/
Virtual RatBrain	Zaborszky *et al.*	http://www.ratbrain.org/
CCDB	Martone *et al.*	http://ccdb.ucsd.edu

2. Virtual Rat Brain Project (Zaborszky et al., 2005a; http://www.ratbrain.org/)

The *software architecture* is based on the NetBeans platform, which provides a modular component framework for Java applications. Layered on top of this are library modules for connecting to the database, dealing with MorphML, and viewing 3D data. The top layer is a collection of applications for warping and submitting data to the database, browsing database contents, and performing analysis on multiple data sets. Figure 20.9 shows the system architecture that consists of three major entities: (a) *the contributor* who does the data acquisition and registers the data into a standardized

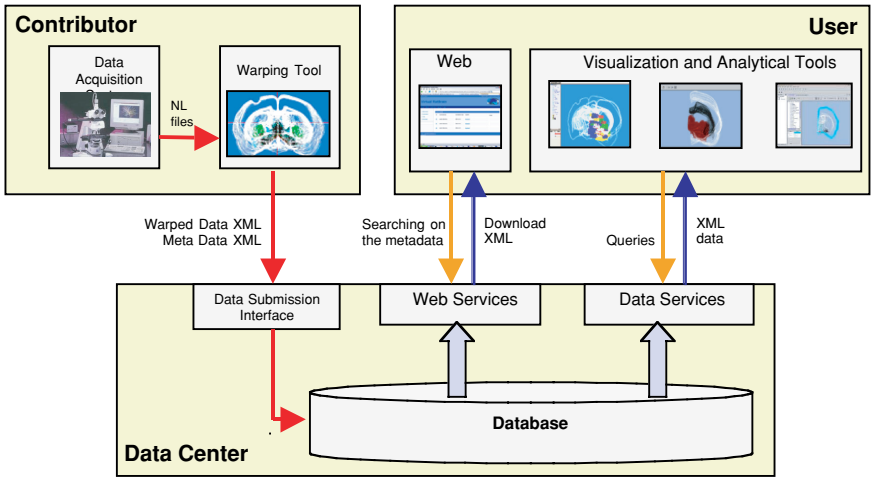

Figure 20.9. System architecture of the Virtual Rat Brain Project. For more details, see at website www.ratbrain.org.

coordinate space (reference brain) by using a special software (warping tool) and uploads it to the database; (b) *the data center* that stores and provides data services to the user; and (c) *the user* who access the data by using the analytical and visualization tools or web browser.

The *warping tool* was created to register data sets into a common coordinate space. The GUI was designed for easy spatial navigation and spatial point selection (Fig. 20.10). The loaded data sets are visualized in a 3D window. The program generates and visualizes three transparent normal section planes that give the basis of the spatial navigation. The user can move these planes along the x, y, and z axes and define points where the planes intersect. The GUI contains three additional 2D windows designed to show "virtual slices" corresponding to each plane. The registration process begins by loading the reference brain (from the database) and the data set to be warped (from the local disk) into the same 3D space. Then the user can define reference points in his/her data set and corresponding points in the reference brain. When all the reference point pairs are defined, the program creates an affine transformation and applies it to the experimental data set on user demand. The result of the action is a new separate data file that contains the experimental data transformed into the standard coordinate space of the reference brain. At the end of the warping procedure, the user is allowed to add descriptive data to the new data set. The tool is able to save the generated data on the local disk as well as upload it to the database. The tool is able to upload original, transformed, and descriptive data. The program currently supports MicroBrightField's Neurolucida files and MDPlot's Accustage files.

The *overlapping analysis tool* (Fig. 20.11) is suited to compare density and overlap between two or more cell populations. The program divides the

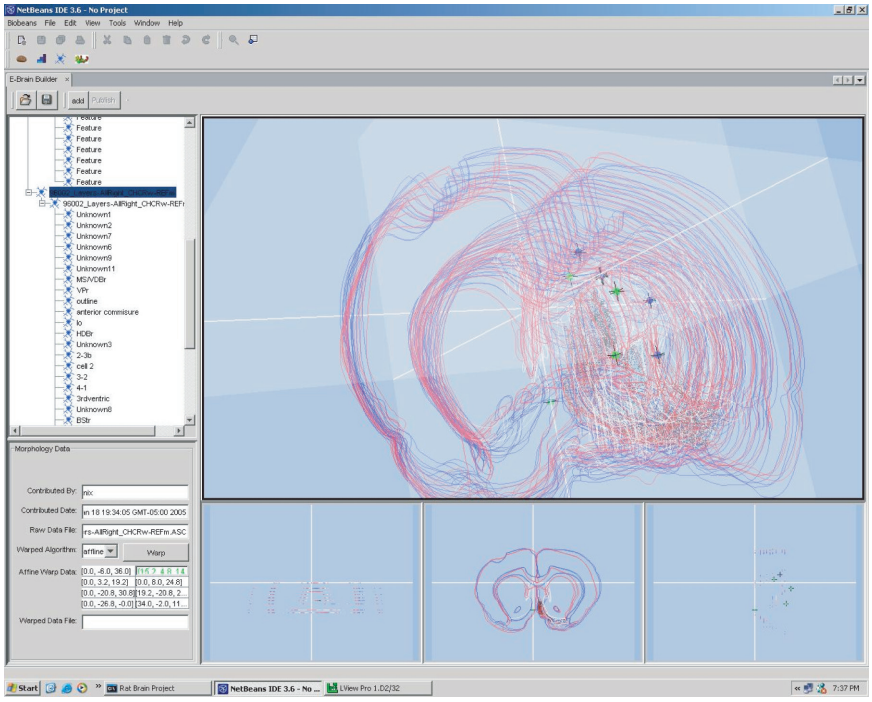

Figure 20.10. The warping tool is used for registering data onto the reference brain and submitting it to the database. Corresponding points for a newly acquired data set and the reference contours can be selected and used to construct a mapping function.

whole brain volume occupied by the data sets into boxes (bins, voxels) of a given size and counts the cell types within each box. If the cell number of each population within a box are equal to or above a certain threshold, the program shows this box in a different color indicating the spatial segregation or overlap. The user selects which cell populations to analyze. The program also makes density measurements comparing the cell numbers from different populations in each box. The program can open multiple data files for cross-brain analyses. A similar approach has been used by Alloway *et al.* (1999) and Leergaard *et al.* (2000). There are several outputs of the program including visualization of bin distributions and summarized cell and bin numbers in table and Microsoft® Excel format (Fig. 20.12; http://www.ratbrain.org/modules/Tools/).

C. Cross-Correlation Function

Consider spike processes as oscillations. Then, the temporal interaction between two cells can be captured as coherent oscillation of the two spike processes, which is quantified by cross-correlation and cross-coherence

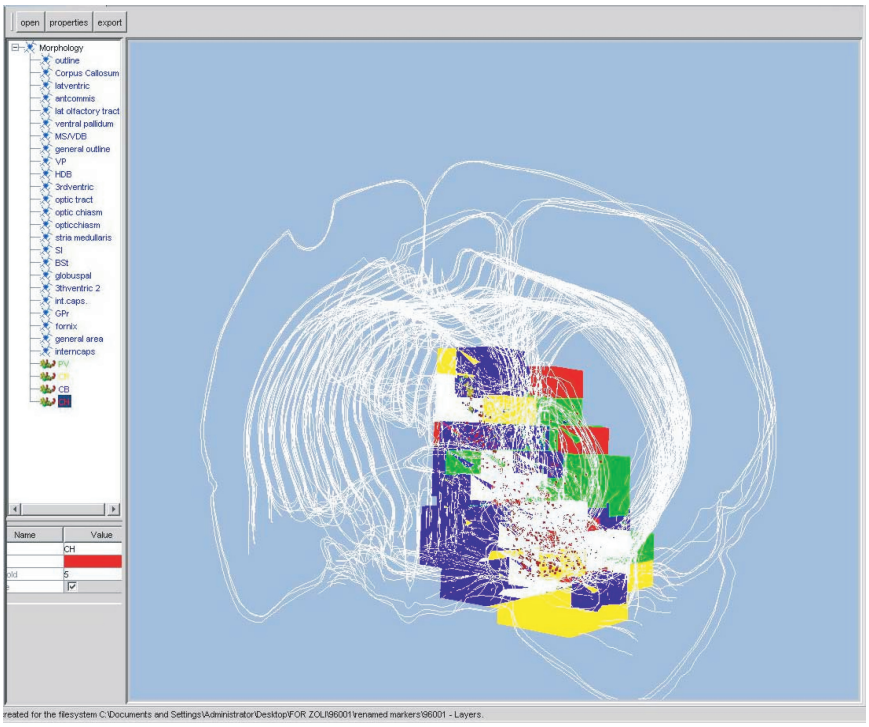

Figure 20.11. The overlap analysis tool allows comparison of overlap of population data sets. The tree display on the left shows named features in the reference brain and reference markers used for warping. The color of the bins is determined by the cell type that is represented by the highest number in the particular bin. Red: cholinergic; blue: calbindin; yellow: calretinin; green: parvalbumin; white: overlapping bins.

functions. The simple cross-correlation function is the product of two spike processes r_1 and r_2 with different time lags τ applied within a time window of stimulus or behavioral event S at time t:

$$CC_{12S}(\tau) = \langle r_{1S}(t+\tau) r_{2S}(t) \rangle_t. \tag{20.7}$$

Since part of the coherent oscillations derive from stimulus induced nonstationarities of the firing rate, in practice we normalize the cross-correlation function by the shift predictor to get a shift-predictor-corrected cross-correlation function:

$$CC_{12S}(\tau) = \langle r_{1S}(t+\tau) r_{2S}(t) - m_{1S}(t+\tau) m_{2S}(t) \rangle_t, \tag{20.8}$$

where m_{1S} and m_{2S} are the mean responses of the two neurons for stimulus S at time t. The stimulus-condition-independent component of cross-correlation can be obtained by averaging CC over S:

$$CC_{12}(\tau) = \langle CC_{12S}(t) \rangle_s. \tag{20.9}$$

A

Bin Type	Boxes	CH cells	CR cells
Empty (with cells)	3	1	2
CH	8	64	1
CR	16	3	104
Overlap	6	26	43
Undefined	0	0	0
Sum	33	94	150

B

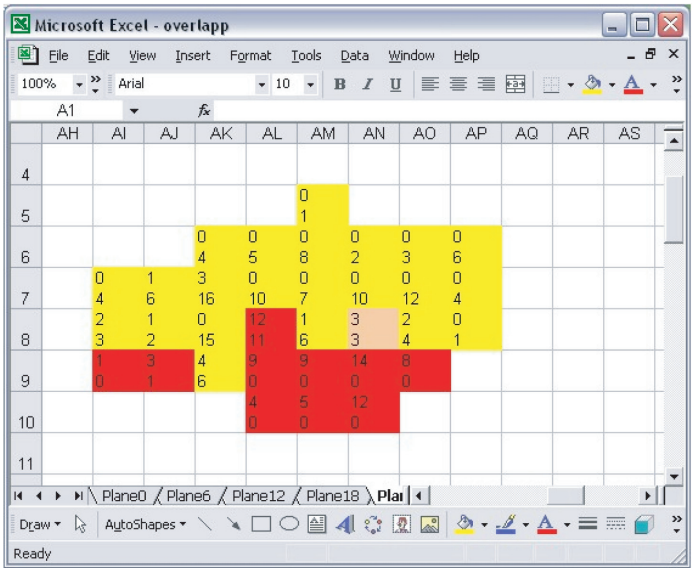

Figure 20.12. The outputs of the overlapping analysis tools in Excel format. (A) The table shows the bin numbers and the occupying cell numbers from a section. (B) The colored table shows the spatial distribution of the bins from the same section. The color of the bins is determined by the cell type that is represented by the highest number in the particular bin. This example is from the basal forebrain (horizontal limb of the diagonal band nucleus), and shows the locations in which the majority of cells are cholinergic (CH, red) or calretinin-containing (CR, yellow). In each bin the upper number represents the cholinergic cells and the lower number the calretinin-containing neurons. Beige: both cell types are represented by an equal number.

For the interpretation of cross-correlation function, see the text (see section "Reconstruction of Functional Connectivity").

ACKNOWLEDGMENTS. We thank Grant Mulliken and Rajan Bhattacharyya for valuable comments and suggestions and thank Peter Bartho for providing figure components for Fig. 20.8. The development of the "Virtual Rat Brain Project" was supported by NIH/NINDS grant NS023945 to Laszlo Zaborszky and funding from UK research councils (MRC and BBSRC) under

the eScience program to Fred W. Howell. We are thankful to Peter Varsanyi and Ms. Nicola McDonnell for the database development.

REFERENCES

Abeles, M., and Gat, I., 2001, Detecting precise firing sequences in experimental data, *J. Neurosci. Methods* **107**(1–2):141–154; Erratum in *J. Neurosci. Methods* **112**(2):203.

Abeles, M., and Gerstein, G. L., 1988, Detecting spatiotemporal firing patterns among simultaneously recorded single neurons, *J. Neurophysiol.* **60**(3):909–924.

Abeles, M., and Goldstein, M. 1977, Multispike train analysis, *Proc. IEEE* **65:**762–773.

Aertsen, A. M., Gerstein, G. L., Habib, M. K., and Palm, G., 1989, Dynamics of neuronal firing correlation: modulation of "effective connectivity," *J. Neurophysiol.* **61**(5):900–917.

Aika, Y., Ren, J. Q., Kosaka, K., and Kosaka, T., 1994, Quantitative analysis of GABA-like-immunoreactive and parvalbumin-containing neurons in the CA1 regions of the rat hippocampus using a stereological method, the dissector, *Exp. Brain Res.* **99:**267–276.

Allman, J. M. 1998, *Evolving Brains*, New York: Scientific American Library, W. H. Freeman and Co.

Alloway, K. D., Crist, J., Mutic, J. J., and Roy, S. A., 1999, Corticostriatal projections from rat barrel cortex have an anisotropic organization that correlates with vibrissal whisking behavior, *J. Neurosci.* **19**(24):10908–10922.

Baker, S. N., Spinks, R., Jackson, A., and Lemon, R. N., 2001, Synchronization in monkey motor cortex during a precision grip task: I. Task-dependent modulation in single-unit synchrony, *J. Neurophysiol.* **85**(2):869–885.

Barbas, H., and Rempel-Clower, N., 1997, Cortical structure predicts the pattern of corticocortical connections, *Cereb. Cortex* **7**(7):635–646.

Bartho, P., Hirase, H., Monconduit, L., Zugaro, M., Harris, K. D., and Buzsaki, G., 2004, Characterization of neocortical principal cells and interneurons by network interactions and extracellular features, *J. Neurophysiol.* **92**(1):600–608.

Binzegger, T., Douglas, R. J., and Martin, K. A. C., 2004, A quantitative map of the circuit of cat primary visual cortex, *J. Neurosci.* **24**(39):8441–8453.

Bower, J. M., and Beeman, D., 1998, *The Book of GENESIS: Exploring Realistic Neural Models with the General Neural Simulation System*, 2nd ed., New York: Springer-Verlag.

Brecht, M., Fee, M. S., Garaschuk, O., Helmchen, F., Margrie, T. W., Svoboda, K., and Osten, P., 2004, Novel approaches to monitor and manipulate single neurons in vivo, *J. Neurosci.* **24:**9223–9227.

Brovelli, A., Ding, M., Ledberg, A., Chen, Y., Nakamura, R., and Bressler, S. L., 2004, Beta oscillations in a large-scale sensorimotor cortical network: directional influences revealed by Granger causality, *Proc. Natl. Acad. Sci. U. S. A.* **101**(26):9849–9854.

Budd, J. M., and Kisvarday, Z. F., 2001, Local lateral connectivity of inhibitory clutch cells in layer 4 of cat visual cortex (area 17), *Exp. Brain Res.* **140**(2):245–250.

Buzsaki, G., 2004, Large-scale recording of neuronal ensembles, *Nat. Neurosci.* **7**(5):446–451.

Buzsaki, G., Penttonen, M., Nadasdy, Z., and Bragin, A., 1996, Pattern and inhibition-dependent invasion of pyramidal cell dendrites by fast spikes in the hippocampus in vivo, *Proc. Natl. Acad. Sci. U. S. A.* **93**(18):9921–9925.

Chen-Bee, C. H., Polley, D. B., Brett-Green, B., Prakash, N., Kwon, M. C., and Frostig, R. D., 2000, Visualizing and quantifying evoked cortical activity assessed with intrinsic signal imaging, *J. Neurosci. Methods* **97**(2):157–173.

Chevalier, G., and Mana, S., 2000, Honeycomb-like structure of the intermediate layers of the rat superior colliculus, with additional observations in several other mammals: AChE patterning, *J. Comp. Neurol.* **419**(2):137–153.

Claverol, E., and Nadasdy, Z., 2004, Intersection of microwire electrodes with proximal CA1 stratum-pyramidal neurons at insertion for multiunit recordings predicted by a 3-D computer model, *IEEE Trans. Biomed. Eng.* **51**(12):2211–2216.

Coogan, T. A., and Burkhalter, A., 1993, Hierarchical organization of areas in rat visual cortex, *J. Neurosci.* **13**(9):3749–3772.

Csicsvari, J., Henze, D. A., Jamieson, B., Harris, K. D., Sirota, A., Bartho, P., Wise, K. D., and Buzsaki, G., 2003, Massively parallel recording of unit and local field potentials with silicon-based electrodes, *J. Neurophysiol.* **90**(2):1314–1323.

Das, A., and Gilbert, C. D., 1995, Long-range horizontal connections and their role in cortical reorganization revealed by optical recording of cat primary visual cortex, *Nature* **375**(6534):780–784.

Das, A., and Gilbert, C. D., 1999, Topography of contextual modulations mediated by short-range interactions in primary visual cortex, *Nature* **399**(6737):655–661.

Destexhe, A., and Babloyantz, A., 1993, A model of the inward current Ih and its possible role in thalamocortical oscillations, *Neuroreport* **4**(2):223–226.

Douglas, R., Martin, K., and Witteridge, D., 1989, A canonical microcircuit for neocortex. *Neural. Comput.* **1:**480–488.

Fee, M. S., Mitra, P. P., and Kleinfeld, D., 1996, Automatic sorting of multiple unit neuronal signals in the presence of anisotropic and non-Gaussian variability, *J. Neurosci. Methods* **69**(2):175–188; Erratum in *J. Neurosci. Methods* **71**(2):233.

Felleman, D. J., and Van Essen, D. C., 1991, Distributed hierarchical processing in the primate cerebral cortex. *Cereb. Cortex* **1**:1–47.

Fiala, J. C., and Harris, K. M., 2001, Extending unbiased stereology of brain ultrastructure to three-dimensional volumes, *J. Am. Med. Inform. Assoc.* **8**(1):1–16.

Földy, C., Dyhrfjeld-Johnsen, J., and Soltesz, I., 2005, Structure of cortical microcircuit theory, *J. Physiol.* **562.1:**47–54.

Freeman, W. J., 2000, Mesoscopic neurodynamics: from neuron to brain, *J. Physiol. (Paris)* **94**(5–6):303–322.

Freund, T. F., and Buzsaki, G., 1996, Interneurons of the hippocampus, *Hippocampus* **6**(4):347–470.

Frostig, R. D., Frostig, Z., and Harper, R. M., 1990, Recurring discharge patterns in multiple spike trains: I. Detection, *Biol. Cybern.* **62**(6):487–493.

Fukuda, T., and Kosaka, T., 2000, Gap junctions linking the dendritic network of GABAergic interneurons in the hippocampus, *J. Neurosci.* **20**(4):1519–1528.

Gerfen, C. R., 1985, The neostriatal mosaic: I. Compartmental organization of projections from the striatum to the substantia nigra in the rat, *J. Comp. Neurol.* **236**(4):454–476.

Gibson, J. R., Beierlein, M., and Connors, B. W., 1999, Two networks of electrically coupled inhibitory neurons in neocortex, *Nature* **402**(6757):75–79.

Gilbert, C. D., 1983, Microcircuitry of the visual cortex, *Annu. Rev. Neurosci.* **6:**217–247.

Gilbert, C. D., and Wiesel, T. N., 1983, Functional organization of the visual cortex. *Prog. Brain Res.* **58:**209–218.

Goldman, P. S., and Nauta, W. J., 1977, Columnar distribution of cortico-cortical fibers in the frontal association, limbic, and motor cortex of the developing rhesus monkey, *Brain Res.* **122**(3):393–413.

Goldman-Rakic, P. S., 1984, Modular organization of prefrontal cortex, *Trends Neurosci.* **7**:419–429.

Granger, C. W. J., 1969, Investigating causal relations by econometric methods and cross-spectral methods, *Econometrica*, **34**:424–438.

Graybiel, A. M., and Ragsdale, C. W., Jr., 1978, Histochemically distinct compartments in the striatum of human, monkeys, and cat demonstrated by acetylthiocholinesterase staining, *Proc. Natl. Acad. Sci. U. S. A.* **75**(11):5723–5726.

Grinvald, A., and Hildesheim, R., 2004, VSDI: a new era in functional imaging of cortical dynamics, *Nat. Rev. Neurosci.* **5**(11):874–885.

Gupta, A., Wang, Y., and Markram, H., 2000, Organizing principles for a diversity of GABAergic interneurons and synapses in the neocortex, *Science* **287**(5451):273–278.

Harris, K. D., Csicsvari, J., Hirase, H., Dragoi, G., and Buzsaki, G., 2003, Organization of cell assemblies in the hippocampus, *Nature* **424**(6948):552–556.

Harris, K. D., Henze, D. A., Csicsvari, J., Hirase, H., and Buzsaki, G., 2000, Accuracy of tetrode spike separation as determined by simultaneous intracellular and extracellular measurements, *J. Neurophysiol.* **84**(1):401–414.

He, W., Hamilton, T. A., Cohen, A. R., Holmes, T. J., Pace, C., Szarowski, D. H., Turner, J. N., and Roysam, B., 2003, Automated three-dimensional tracing of neurons in confocal and brightfield images, *Microsc. Microanal.* **9**(4):296–310.

Hebb, D. O., 1949, *Organization of Behavior*, New York: Wiley.

Henze, D. A., Borhegyi, Z., Csicsvari, J., Mamiya, A., Harris, K. D., and Buzsaki, G., 2000, Intracellular features predicted by extracellular recordings in the hippocampus in vivo, *J. Neurophysiol.* **84**(1):390–400.

Hines, M. L., and Carnevale, N. T., 1997, The NEURON simulation environment, *Neural Comput.* **9:**1179–1209.

Hubel, D. H., and Wiesel, T. N., 1959, Receptive fields of single neurones in the cat's striate cortex, *J. Physiol.* **148:**574–591.

Hubel, D. H., and Wiesel, T. N., 1972, Laminar and columnar distribution of geniculo-cortical fibers in the macaque monkey, *J. Comp. Neurol.* **146**(4):421–450.

Ikegaya, Y., Aaron, G., Cossart, R., Aronov, D., Lampl, I., Ferster, D., and Yuste, R., 2004, Synfire chains and cortical songs: temporal modules of cortical activity, *Science* **304**(5670): 559–564.

Isseroff, A., Schwartz, M. L., Dekker, J. J., and Goldman-Rakic, P. S., 1984, Columnar organization of callosal and associational projections from rat frontal cortex, *Brain Res.* **293**(2):213–223.

Johnson, R. R., and Burkhalter, A., 1997, A polysynaptic feedback circuit in rat visual cortex, *J. Neurosci.* **17**(18):7129–7140.

Kalisman, N., Silberberg, G., and Markram, H., 2005, The neocortical microcircuit as a tabula rasa, *Proc. Natl. Acad. Sci. U. S. A.* **102**(3):880–885.

Kaminski, M., Ding, M., Truccolo, W. A., and Bressler, S. L., 2001, Evaluating causal relations in neural systems: granger causality, directed transfer function and statistical assessment of significance, *Biol. Cybern.* **85**(2):145–157.

Kaminski, M. J., and Blinowska, K. J., 1991, A new method of the description of the information flow in the brain structures, *Biol. Cybern.* **65:**203–210.

Kemere, C., Shenoy, K. V., and Meng, T. H., 2004, Model-based neural decoding of reaching movements: a maximum likelihood approach, *IEEE Trans. Biomed. Eng.* **51**(6):925–932.

Kisvarday, Z. F., Ferecsko, A. S., Kovacs, K., Buzas, P., Budd, J. M., and Eysel, U. T., 2002, One axon-multiple functions: specificity of lateral inhibitory connections by large basket cells, *J. Neurocytol.* **31**(3–5):255–264.

Koralek, K. A., Olavarria, J., and Killackey, H. P., 1990, Areal and laminar organization of corticocortical projections in the rat somatosensory cortex, *J. Comp. Neurol.* **299**(2):133–150.

Kötter, R., Hilgetag, C. C., and Stephan, K. E., 2001, Connectional characteristics of areas in Walker's map of prefrontal cortex, *Neurocomputing* **38–40**:741–746.

Lee, A. K., and Wilson, M. A., 2002, Memory of sequential experience in the hippocampus during slow wave sleep, *Neuron* **36**(6):1183–1194.

Leergaard, T. B., Alloway, K. D., Mutic, J. J., and Bjaalie, J. G., 2000, Three-dimensional topography of corticopontine projections from rat barrel cortex: correlations with corticostriatal organization, *J. Neurosci.* **20**(22):8474–8484.

Leise, E. M. 1990, Modular construction of nervous system: a basic principle of design for invertebrates and vertebrates, *Brain Res. Rev.* **15:**1–23.

Lewicki, M. S., 1998, A review of methods for spike sorting: the detection and classification of neural action potentials, *Network* **9**(4):R53–R78 (Review).

Li, W., and Gilbert, C. D., 2002, Global contour saliency and local collinear interactions, *J. Neurophysiol.* **88**(5):2846–2856.

Lubke, J., Egger, V., Sakmann, B., and Feldmeyer, D., 2000, Columnar organization of dendrites and axons of single and synaptically coupled excitatory spiny neurons in layer 4 of the rat barrel cortex, *J. Neurosci.* **20**(14):5300–5311.

Maccaferri, G., and Lacaille, J. C., 2003, Interneuron diversity series: hippocampal interneuron classifications—making things as simple as possible, not simpler, *Trends Neurosci.* **26:**564–571.

Malach, R., 1994, Cortical columns as devices for maximizing neuronal diversity, *Trends Neurosci.* **17**(3):101–104 (Review).

Malmierca, M. S., Leergaard, T. B., Bajo, V. M., Bjaalie, J. G., and Merchan, M. A., 1998, Anatomic evidence of a three-dimensional mosaic pattern of tonotopic organization in the ventral complex of the lateral lemniscus in cat, *J. Neurosci.* **18**(24):10603–10618.

Mountcastle, V. B., 1957, Modality and topographic properties of single neurons of cat's somatic sensory cortex, *J. Neurophysiol.* **20**(4):408–434.

Mountcastle, V. B., 1998, *Perceptual Neuroscience: The Cerebral Cortex*, Harvard University Press, Cambridge, MA.

Musallam, S., Corneil, B. D., Greger, B., Scherberger, H., and Andersen, R. A., 2004, Cognitive control signals for neural prosthetics, *Science*, **305**(5681):258–262.

Nadasdy, Z., 2000, Time sequences and their consequences, *J. Physiol. (Paris)* **94:**505–524.

Nadasdy, Z., Csicsvari, J., Penttonen, M., Hetke, J., Wise, K., and Buzsáki, G., 1998, Extracellular recording and analysis of neuronal activity: from single cells to ensembles, In: Eichenbaum, H. B., and Davis, J. L. (eds.), *Neuronal Ensembles: Strategies for Recording and Decoding*, New York: Wiley.

Nadasdy, Z., Hirase, H., Czurko, A., Csicsvari, J., and Buzsaki, G., 1999, Replay and time compression of recurring spike sequences in the hippocampus, *J. Neurosci.* **19**(21):9497–9507.

Nadasdy, Z., and Zaborszky, L., 2001, Visualization of density relations in large-scale neural networks, *Anat. Embryol. (Berl.)* **204**(4):303–317.

Nordhausen, C. T., Maynard, E. M., and Normann, R. A., 1996, Single unit recording capabilities of a 100 microelectrode array, *Brain Res.* **726**(1–2):129–140.

Ohki, K., Chung, S., Ch'ng Y. H., Kara, P., and Reid, R. C., 2005, Functional imaging with cellular resolution reveals precise micro-architecture in visual cortex, *Nature* **433**(7026):597–603.

Palm, G., Aertsen, A. M., and Gerstein, G. L., 1988, On the significance of correlations among neuronal spike trains, *Biol. Cybern.* **59**(1):1–11.

Paperna, T., and Malach, R., 1991, Patterns of sensory intermodality relationships in the cerebral cortex of the rat, *J. Comp. Neurol.* **308**(3):432–456.

Peters, A., and Feldman, M. L., 1976, The projection of the lateral geniculate nucleus to area 17 of the rat cerebral cortex: I. General description, *J. Neurocytol.* **5:**63–84.

Peters, A., and Payne, B. R., 1993, Numerical relationships between geniculocortical afferents and pyramidal cell modules in cat primary visual cortex. *Cereb. Cortex* **3:**69–78.

Pouille, F., and Scanziani, M., 2004, Routing of spike series by dynamic circuits in the hippocampus, *Nature* **429**(6993):717–723.

Prinz, A. A., Bucher, D., and Marder, E., 2004, Similar network activity from disparate circuit parameters, *Nat. Neurosci.* **7**(12):1287–1288.

Pucak, M. L., Levitt, J. B., Lund, J. S., and Lewis, D. A., 1996, Patterns of intrinsic and associational circuitry in monkey prefrontal cortex, *J. Comp. Neurol.* **376**(4):614–630.

Quian-Quiroga, R., Nadasdy, Z., and Ben-Shaul, Y., 2004, Unsupervised spike detection and sorting with wavelets and superparamagnetic clustering, *Neural Comput.* **16**(8):1661–1687.

Rakic, P., 1995, Radial versus tangential migration of neuronal clones in the developing cerebral cortex, *Proc. Natl. Acad. Sci. U. S. A.* **92**(25):11323–11327.

Rempel-Clower, N. L., and Barbas, H., 2000, The laminar pattern of connections between prefrontal and anterior temporal cortices in the Rhesus monkey is related to cortical structure and function, *Cereb. Cortex* **10**(9):851–865.

Rockland, K. S., 1998, Complex microstructures of sensory cortical connections, *Curr. Opin. Neurobiol.* **8**(4):545–551 (Review).

Rodriguez, A., Ehlenberger, D., Kelliher, K., Einstein, M., Henderson, S. C., Morrison, J. H., Hof, P. R., and Wearne, S. L., 2003, Automated reconstruction of three-dimensional neuronal morphology from laser scanning microscopy images, *Methods* **30**(1):94–105.

Somogyi, P., and Klausberger, T., 2005, Defined types of cortical interneurone structure space and spike timing in the hippocampus, *J. Physiol. (London)* **562:**9–26.

Somogyi, P., Tamas, G., Lujan, R., and Buhl, E. H., 1998, Salient features of synaptic organisation in the cerebral cortex. *Brain Res. Brain Res. Rev.* **26**(2–3):113–135.

Sporns, O., and Kötter, R., 2004, Motifs in brain networks, *PLoS Biol.* **2**(11):e369.

Stepanyants, A., Hof, P. R., and Chklovskii, D. B., 2002, Geometry and structural plasticity of synaptic connectivity, *Neuron* **34**(2):275–288.

Stepanyants, A., Tamas, G., and Chklovskii, D. B., 2004, Class-specific features of neuronal wiring, *Neuron* **43**(2):251–259.

Szentagothai, J., 1978, The neuron network of the cerebral cortex: a functional interpretation. *Proc. R. Soc. Lond. B.* **201:**219–248.

Szentagothai, J., 1983, The modular architectonic principle of neural centers, *Rev. Physiol. Biochem. Pharmacol.* **98:**11–61.

Tamas, G., Buhl, E. H., Lorincz, A., and Somogyi, P., 2000, Proximally targeted GABAergic synapses and gap junctions synchronize cortical interneurons, *Nat. Neurosci.* **3**(4):366–371.

Tamas, G., Buhl, E. H., and Somogyi, P., 1997, Massive autaptic self-innervation of GABAergic neurons in cat visual cortex, *J. Neurosci.* **17**(16):6352–6364.

Traub, R. D., Jefferys, J. G. R., and Whittington, M. A., 1999, *Fast Oscillations in Cortical Circuits*, Bradford Books, MIT Press, Cambridge, MA.

Vetter, R. J., Williams, J. C., Hetke, J. F., Nunamaker, E. A., and Kipke, D. R., 2004, Chronic neural recording using silicon-substrate microelectrode arrays implanted in cerebral cortex, *IEEE Trans. Biomed. Eng.* **51**(6):896–904.

Vreeswijk, C. V., 1996, Partial synchronization in populations of pulse-coupled oscillators, *Phys. Rev. E Stat. Phys. Plasmas Fluids Relat. Interdiscip. Topics* **54**(5):5522–5537.

Wang, X. J., and Rinzel, J., 1993, Spindle rhythmicity in the reticularis thalami nucleus: synchronization among mutually inhibitory neurons, *Neuroscience* **53**(4):899–904.

Watts, J., and Thomson, A. M., 2005, Excitatory and inhibitory connections show selectivity in the neocortex, *J. Physiol. (London)* **562:**89–97.

Wickelgren, W. A., 1999, Webs, cell assemblies, and chunking in neural nets: introduction, *Can. J. Exp. Psychol.* **53**(1):118–131.

Yoshimura, Y., Dantzker, J. L., and Callaway, E. M., 2005, Excitatory cortical neurons form fine-scale functional networks, *Nature* **433**(7028):868–873.

Yuste, R., and Denk, W., 1995, Dendritic spines as basic functional units of neuronal integration, *Nature* **375**(6533):682–684.

Zaborszky, L., 2002, The modular organization of brain systems. Basal forebrain: the last frontier, *Prog. Brain Res.* **136:**359–372.

Zaborszky, L., Buhl, D. L., Pobalashingham, S., Bjaalie, J. G., and Nadasdy, Z., 2005b, Three-dimensional chemoarchitecture of the basal forebrain: spatially specific association of cholinergic and calcium binding protein-containing neurons, *Neuroscience*, **136**(3):697–713.

Zaborszky, L., Csordas, A., Buhl, D. L., Duque, A., Somogyi, J., and Nadasdy, Z., 2002, Computational anatomical analysis of the basal forebrain corticopetal system, In: Ascoli, G. A. (ed.), *Computational Neuroanatomy: Principles and Methods*, New Jersey: Humana Press.

Zaborszky, L., Varsanyi, P., Mc Donnell, N. C., and Howell, F. W., 2005a, 3D cellular database of the rat brain: integrated anatomical data, *Soc. Neurosci. Abstr.* **31**.

Zaborszky, L., and Wolff, J. R., 1982, Distribution patterns and individual variations of callosal connections in the albino rat, *Anat. Embryol. (Berlin)* **165**(2):213–232.

Zhang, K., Ginzburg, I., McNaughton, B. L., and Sejnowski, T. J., 1998, Interpreting neuronal population activity by reconstruction: unified framework with application to hippocampal place cells, *J. Neurophysiol.* **79**(2):1017–1044.